STANFORD RESEARCH INSTITUTE
MENLO PARK, CALIFORNIA

July 31, 1967

Final Report | July 1, 1966 to June 30, 1967

CORRELATION BETWEEN SOLID PROPELLANT MECHANICAL PROPERTIES AND EXPLOSION EFFECTS

Prepared for:

CHIEF, SOLID PROPULSION TECHNOLOGY PROGRAMS
CODE RPS, OART
NATIONAL AERONAUTICS AND SPACE ADMINISTRATION
WASHINGTON, D. C.

CONTRACT NO. NAS7-480
CONTROL NO. PR 66-237

By: A. B. AMSTER, R. W. WOOLFOLK, AND G. M. MULLER

Contributors: J. M. GORFINKEL, STANFORD RESEARCH INSTITUTE
G. E. DUVALL AND L. D. BERTHALF, WASHINGTON STATE UNIVERSITY

SRI Project FRU-6150

Approved: A. G. BROWN, DIRECTOR
CHEMISTRY & CHEMICAL ENGINEERING LABORATORY

Copy No. 22

ABSTRACT

This is the final report of work on Contract NAS7-480, covering the period July 1, 1966 to June 30, 1967, to study the relation between solid propellant mechanical properties and explosion effects. For a selected geometry an imposed shock decays exponentially. Only a very small fraction of the propellant lost in the model blast contributes to the blast wave, and flash radiographs show an anomalous structure of the pressure wave traveling through the propellant. Several points on the Hugoniot of the selected propellant have been obtained, but these do not account for this anomaly.

CONTENTS

ILLUSTRATIONS

ILLUSTRATIONS
(Continued)

TABLES

INTRODUCTION

Rocket systems which have been planned may incorporate millions of pounds of solid propellant. Furthermore, thermochemically, solid propellants are practically indistinguishable from explosives in that they have comparable heats of reaction. Consequently, it is quite proper that the explosive properties of large solid propellant motors be carefully examined.

Fortunately, the hazard situation is not so bleak as some imagined. It has been established[1] beyond reasonable doubt that conventional solid motors* do not detonate in diameters less than 20 inches, and there is evidence that the true failure diameter for detonation is larger, perhaps considerably so. Even above the failure diameter, exceedingly strong shocks may be required to initiate stable detonation. In conventional jargon, the propellants are insensitive; in fact it is difficult to envision realistic conditions which would lead to detonation. On the other hand, solid propellant motors have been known to explode, causing considerable damage--though much less than would accompany complete detonation.

The effects of stable detonation are predictable with accuracy sufficient for safety engineering.[2] However, the far more likely nondetonative explosions consume as yet unpredictable amounts of propellant, and thus, the accompanying blast effects are also not predictable.

---

*In this context, these incorporate propellants consisting mainly of ammonium perchlorate and aluminum in a rubbery binder; no explosives are included among the ingredients. These are the only type propellant considered in this report.

The explosion of a nondetonable but normally burning propellant purportedly results from a sequence of events that proceeds approximately as follows:

(a) The propellant is subjected to a strong shock wave and is shattered.

(b) Combustion spreads over the newly formed surfaces.

(c) Because of the very large total surface area the rate of consumption and, hence, of energy release is excessive. Therefore, the pressure increases rapidly within the combustion zone, causing the burning rate to increase.

(d) Finally, the total rate of energy release and the pressure become so great that a blast ensues.

To test the validity of this approach, it is necessary to study the effects of shock waves on propellants and to search for a correlation between these effects and the associated blast waves. It has been the aim of our research to perform this test. Before discussing the manner in which this was done, we review pertinent areas briefly, in the next section. These include: response of solid propellants to strong shocks; attenuation of shock waves in solids; equation of state and plastic-elastic transitions of model solids; and blast contribution of explosive chemical reactions.

In subsequent sections we present a more detailed model and an outline of the studies performed to evaluate the hypothesis, the results of these studies, a discussion of the results and their significance, and lastly, suggestions for additional research.

II GENERAL DISCUSSION

A. Response of Solid Propellants to Strong Shocks

Conventional unidimensional detonation theory suggests that any solid which decomposes exothermally can sustain a suitably initiated stable detonation. In the real tridimensional world a revised theory predicts, and experience confirms, the existence of a failure diameter, i.e., a diameter below which stable detonation is impossible.[3] With certain types of energetic propellants, e.g., those containing nitroglycerine, conventional explosives, etc., this failure diameter is small, perhaps of the order of fractions of a centimeter. Fortunately, for those propellants which we choose to call "conventional" (ammonium perchlorate-rubbery binder-metal powder) and for a sample with a functional integrity, this failure diameter is very large, and strong shocks would probably be required to initiate detonation in even these sizes. However, should the propellant grain be fragmented, burning may spread over the large exposed surface area and become explosively rapid. Though the directed burning rate may be below detonation velocity, the net mass consumption rate may be comparable to that of detonation. There is ample evidence to support the hypothesis that solid propellant explosions can result when a normally burning grain is subjected to a strong shock. This shock, which may originate internally or externally, shatters a portion of the propellant, thus exposing large areas to burning and ultimate explosion.[1]

B. Attenuation of Shock Waves in Solids

A shock wave is characterized as a region of abruptly rising pressure traveling at a velocity which is supersonic with respect to the unshocked medium. To an observer moving with the wave the medium appears to be moving into the wave. The pressure profile is as illustrated in Fig. 1.

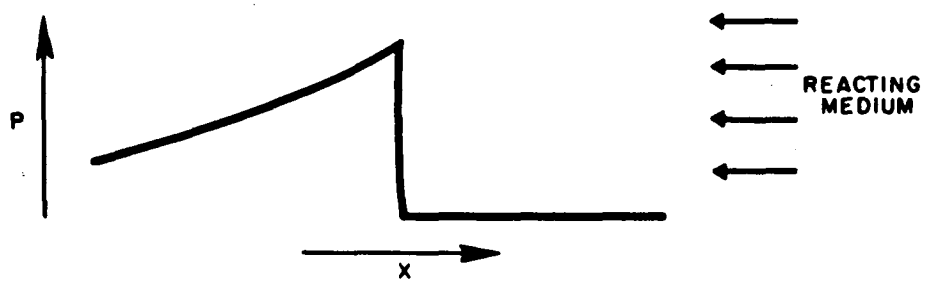

FIG. 1 SHOCK WAVE PRESSURE PROFILE

If the energy is supplied to the wave at a constant rate, the peak pressure remains constant. Detonations represent systems in which the requisite energy is supplied by rapid chemical reaction and the detonation pressure is defined by the stoichiometry and thermodynamics of the reaction and its products. In the absence of chemical reaction (or, for real systems, if the reaction is too slow) the peak pressure decreases with time--often exponentially--and in a very short time and distance decays to a sonic wave. This process apparently occurs in propellants which either are below failure diameter or are subjected to shocks weaker than those required to initiate a stable detonation. Under these circumstances a finite region of the shocked propellant sample will have been subjected to a monotonically decreasing pressure wave. With real samples of a specific

propellant a relatively few experiments will provide the necessary data to define the peak pressure history of any plane beyond that initially shocked. The results for a cylindrical acceptor can be expressed as follows:

$$P_x = P_o e^{-k_x x} \quad \text{or} \quad P_t = P_o e^{-k_t t},$$

where

P_o = incident peak pressure

x = distance from incident plane

t = time elapsed since imposition of shock

k_x, k_t = constants

P_x = peak pressure attained at x

P_t = peak pressure in wave at t.

C. Equation of State and Elastic-Plastic Transitions

The conventional equation of state relates the pressure, volume, and temperature of a system at equilibrium with its environment regardless of its history. For the moment, however, we must be concerned with the Hugoniot equation of state, which describes the states attainable by shocking a sample from a given set of starting conditions, generally ambient pressure and temperature. For final pressures of the order of many tens of kilobars a typical Hugoniot is shown in Fig. 2. The very low pressure portion of the Hugoniot is often linear as exaggerated in Fig. 3.

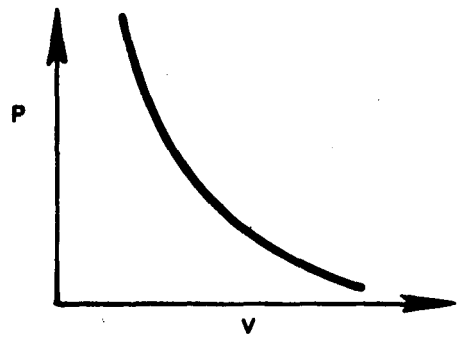

FIG. 2 HUGONIOT (High Pressure)

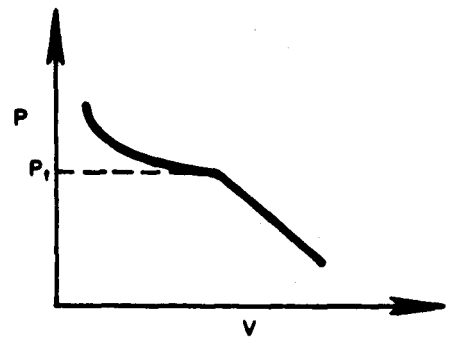

FIG. 3 HUGONIOT (Low Pressure)

The behavior below P_t is characterized as elastic, that above P_t is plastic. In the elastic region deformation is reversible, in the plastic region it is not. Generally P_t is of the order of < 10 kbar. Experiments to determine the general shape of the Hugoniot and the value of P_t for a specific propellant have been developed in recent years (see for example, Charest et al.[4]).

D. Blast Contribution of Explosive Chemical Reactions

Predicting the blast effects of a stable detonation is relatively simple.[2] For moderate accuracy one needs only the heat of explosion of the reactant. In fact, it may be that the scatter in the reported results is attributable to limitations of pressure measurements rather than to limitations of the model. It is convenient to express blast effects in relative terms. Thus, we use the term "TNT equivalent" in mass units to describe any explosion in terms of the mass of TNT required to produce the same effect. In percentage units, TNT equivalent describes

the efficiency of a given explosive. Most chemical explosives have TNT equivalents in the range of 90 to 110%,[5] as do most high energy detonating solid propellants; and for damage predictions, the differences are insignificant.

For nondetonating exploding systems, the fraction consumed by violent reaction is a function of many factors. In these instances TNT equivalence is meaningless except as it relates to a particular system subjected to a particular perturbation. However, it is an interesting speculation that the blast accompanying the explosion of a solid propellant is directly related to the fraction consumed at shock velocity. We can describe an experiment to examine this hypothesis. Assume a strong planar shock wave is imposed upon a cylindrical propellant sample (Fig. 4). Measure both the attenuating velocity of the shock as it travels through the sample and the blast caused by the accompanying explosion. Analysis of the data will locate a hypothetical plane A beyond which (approximately) the propellant does not contribute to the blast. It is to the correlation of this analysis with physical properties that the approach of the next section is directed.

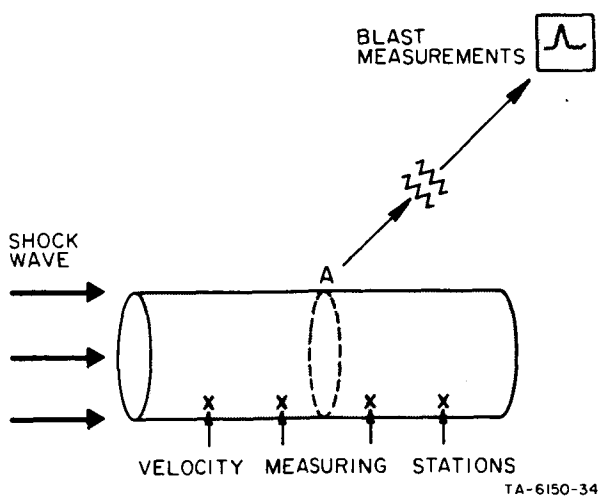

FIG. 4 SHOCK IMPOSING ON SAMPLE

III SCOPE OF RESEARCH

A. Model: Correlation of Blast Damage with Propellant Properties

The pressure of a shock wave passing through a propellant (Fig. 4) can be calculated from the shock velocity and the Hugoniot.[3] Consequently, the pressure-distance behavior of the wave is known. From this, we can determine the distance the wave must travel for the pressure to drop to P_t, the elastic-plastic transition point. This result is then compared with the calculated location of plane A to obtain the answers to the following:

(a) Above what pressure, P_B, must a propellant be shocked to contribute to a distant blast wave?*

(b) How does this pressure, P_B, relate to P_t? The model suggests that $P_B \approx P_t$.

An experimental program was designed to test the feasibility of using this model for broader application.

B. Research Approach

From the foregoing it is apparent that information from different sources was required for the study. For one sample propellant, we must

---

*It is tension not pressure which ruptures the propellant, but the magnitude of the tension is determined by the steepness of the rarefaction following the shock. Presumably this steepness is also defined by the shock amplitude. As pressure can be measured and not rarefaction, it is convenient to relate fragmentation to pressure.

determine (a) the Hugoniot, (b) shock attenuation equations, (c) blast effects accompanying propellant shocking,* and (d) quantity of propellant destroyed by an explosion. Of these, only the Hugoniot is a specific property of the propellant itself. The remainder depend upon test geometry; experiments to obtain the needed information were all performed with one configuration. No particular arrangement has any a priori theoretical advantage. Because of the availability of the donor pellets and because there is considerable information on the behavior of Lucite and/or Plexiglas in the same geometry, we chose to test specimens conforming to the dimensions of the NOL gap test:[1]

Shock donor:	two tetryl pellets, each 2 in. diam x 1 in. thick, density $\approx$ 1.51 g/cc.
Propellant acceptor:	2 in. diam x 4 in. long.

The unreacted Hugoniot can be obtained in a number of different ways--all adequately described elsewhere.[6] Essentially each imposes a plane shock wave on the sample. The particle and shock velocities of the sample are measured using reflected light or aquarium techniques;[7] the hydrodynamic conservation equations are then used to calculate the desired pressure-velocity data. The procedures are relatively simple

---

*We distinguish between blast and shock: (a) The shock wave propagates within the propellant; its source is an explosive donor. (b) The blast wave propagates through the air; its source is the donor plus the propellant. Technically both are shock waves, but this usage is consistent with present jargon.

for pressures above 50 kbar, but become more exacting at lower pressures. The actual methods used are discussed in a later section.

To obtain shock attenuation data a strong shock is imposed on the sample in the test geometry, and electronic techniques are used to measure the time of arrival of the shock at each of several planes in the sample.[7] These data are reduced to equations which relate shock velocity to position and elapsed time.

To obtain the blast data, samples, in the specified geometry, are subjected to the donor shock and gauges arrayed along radii from the charge center. In our experiments, the output of special piezoelectric gauges was recorded and interpreted, directly, as pressure-time data. Other gauges were used to record the arrival time of the blast wave at the gauge position. The blast wave velocities were calculated from the intergauge distances, and the peak pressures were computed from the equation of state for air. The information from these tests is used to compare the effect of the propellant with a comparable quantity of detonating explosive. The comparison is expressed in terms of the donor charge.

After the model explosions the propellant samples were recovered to determine the amount destroyed by the explosion. To supplement the measurements, we also made flash radiographs during some of the explosions.

IV EXPERIMENTAL AND THEORETICAL STUDIES

A. Propellant Selection

It has been the aim of this program to study the blast resulting from the explosion of a "conventional" composite propellant. It is important that the selected propellant have notable batch-to-batch uniformity, especially with regard to mechanical properties, long-term ambient stability and easy machining. On the basis of past experience with many propellants, the formula given in Table I and designated as PBAN-170 was used in all our studies on this program. The density of one batch and the mechanical properties of three specimens from the batch are listed in Table II. The burning rate curve for a typical specimen is shown in Fig. 5.

TABLE I

FORMULA OF PBAN-170

Ingredient	Weight Percent
Ammonium Perchlorate, Unground	44.20
Ammonium perchlorate, avg. diam. 11μ	23.50
Aluminum, V.M.* H-322	15.00
Dioctyl adipate	2.40
PBAN-terpolymer	10.886
Nadic Methyl Anhydride	0.588
Dow epoxy resin 332	2.926
Iron oxide, CKW** R-5098	0.50

*Valley Metallurgical Corporation, Essex, Connecticut.

**C.K. Williams & Company, Easton, Pennsylvania.

TABLE II

PROPERTIES OF PBAN-170

(at ambient temperature)

Density	0.061 lb/in.^{3}		
Specific Gravity	1.69		
	Specimen No.		
Mechanical Property:*	1	2	3
Maximum tensile strength, S_m, psi	114	116	113
Tensile strength at break S_b, psi	89.5	89.7	89.8
Elongation at break	0.59	0.60	0.58
Elongation at maximum tensile strength	0.39	0.43	0.40

*Crosshead Speed, 2 in./min.

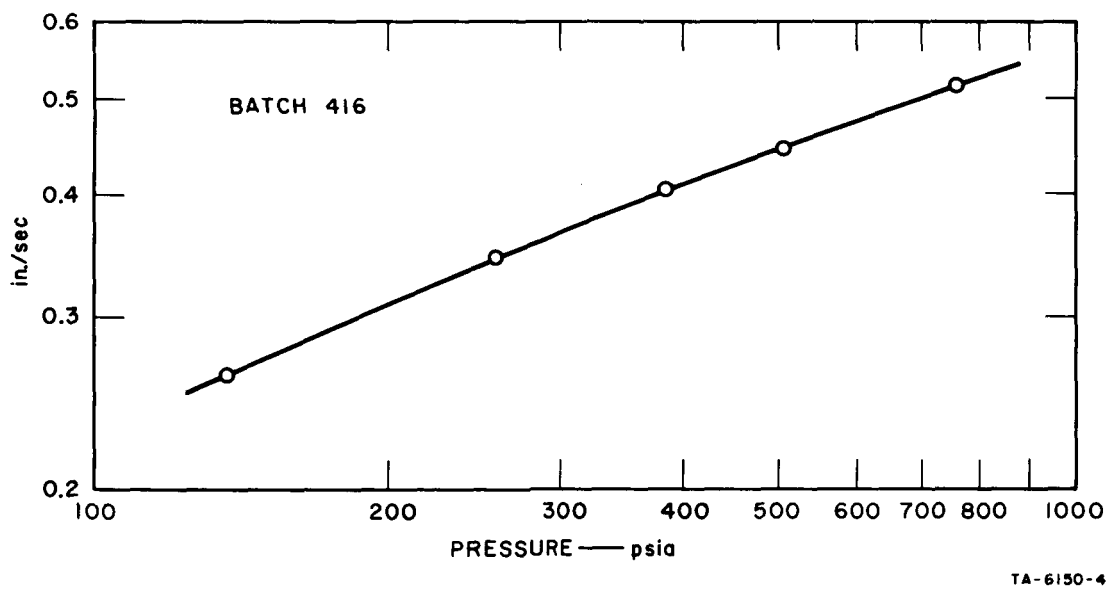

FIG. 5 PBAN-170 BURNING RATE

B. Attenuation of Shock in the Propellant

1. Experimental Procedures

The experimental arrangement shown in Fig. 6 was used to measure the velocity of the decelerating donor shock as it traversed the propellant acceptor. The donor consisted of a pair of tetryl pellets, each 2 inches in diameter by one inch thick, density (nominally) 1.51 g/cc. The acceptor was of PBAN-170, 2 inches in diameter and of specified length.

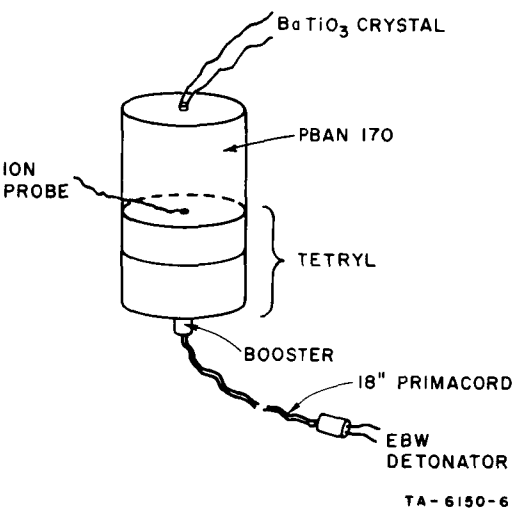

FIG. 6 SHOCK ATTENUATION TEST ARRANGEMENT

The transit time of the donor shock through the propellant was measured with a raster oscilloscope which was triggered when the detonator was initiated. This procedure produced a record of the instant when the shock wave passed the ion probe and when it arrived at the $BaTiO_3$ piezocrystal probe. Time on the raster was resolved accurately to better than 0.05 μsec. Thus each interval, which involved two readings, was accurate to within 0.07 μsec, i.e., $0.07 = (0.05^2 + 0.05^2)^{\frac{1}{2}}$.

A total of 53 shots were made; the results appear in Table III.

TABLE III

SHOCK ATTENUATION DATA

Pellet Thickness mm	Transit Time μsec			
	1	2	3	4
6.60	1.30			
6.76		1.35		
6.86			1.33	
6.88				1.40
13.11	2.60			
13.13		2.55		
13.16			2.70	
13.18				2.60
18.92	3.95			
19.05		3.95		
25.4	5.40	5.45	5.35	5.40
31.75	6.90	7.00	6.90	7.00
38.1	8.48	8.55	8.53	8.60
43.97	10.03			
44.40		10.03		
44.60			10.28	
44.96				10.33
50.8	12.10	12.00	12.05	12.00
63.5	16.15	16.05	16.05	16.23
76.2	20.85	20.60	20.50	20.60
87.50	25.25	24.98		
89.15			25.35	
90.30				25.65
98.68	29.15			
101.45		30.28		
102.62			31.90	
115.21	35.35			
115.42		35.60		
127.41	40.80			
127.69		41.30		
140.26	46.25			
140.84		47.00		
153.04	52.50			
153.16		51.55		

2. Mathematical Analysis*

There is no proven theory to describe the velocity decay of a shock wave in a finite inert cylinder. By analogy with other attenuation phenomena (e.g., light absorption), it is heuristically attractive to postulate an exponential decay law. There is some experimental justification for this and we pursue this approach here.

For the geometry of the attenuation test, let x be the distance that the shock has traveled in time t, let c be the longitudinal sonic velocity in the cylinder, and V, k, and α be constants. The boundary conditions imposed by the physical regime are:

$$\text{for } t = 0 \quad \begin{cases} x = 0, & \text{(1a)} \\ \dot{x} > 0, & \text{(1b)} \\ \ddot{x} < 0, & \text{(1c)} \end{cases}$$

$$\text{for large } t \quad \begin{cases} x \text{ is large } (\sim ct), & \text{(2a)} \\ \dot{x} = c, & \text{(2b)} \\ \ddot{x} = 0. & \text{(2c)} \end{cases}$$

Our assumption is that $\dot{x}$ is of the form:

$$\dot{x} = Ve^{-kt} \qquad \text{(3a)}$$

But, to conform to the requirement (2b) we change this to

$$\dot{x} = Ve^{-kt} + c. \qquad \text{(3b)}$$

---

*Mr. J. Martin Gorfinkel of the Institute's Mathematical Sciences Department aided in the preparation of this section.

Integrating (3b) gives

$$x = -\frac{V}{k} e^{-kt} + ct + \alpha. \tag{4}$$

From (1a), $\alpha = V/k$; therefore,

$$x = -\frac{V}{k} e^{-kt} + ct + \frac{V}{k}. \tag{5}$$

Differentiating (3b) gives

$$\ddot{x} = -kVe^{-kt} \tag{6}$$

Equations (5), (3b), and (6) satisfy the requirements of conditions (1) and (2), to wit:

	x	$\dot{x}$	$\ddot{x}$
$t = 0$	0	$V + c$	$-kV$
large t	$\sim ct$	c	0

Thus, if the hypothesis is correct, the data should fit equation (5).

There is no simple regression formula by which a least squares fit of x and t can be used to evaluate V, k, and c, none of which is known a priori.

However, equation (5) may be written in the form:

$$x = A(1 - e^{-Kt}) + Bt \tag{7}$$

where A, B and K are constants. If it is assumed that x is observed with some error, then we can write

$$x_o = A(1 - e^{-Kt}) + Bt + \epsilon \tag{8}$$

where ϵ is an error term and x_o is the observed value of x.

We want to find A, B, and K to minimize

$$\Sigma\left\{x - [A(1 - e^{-Kt}) + Bt]\right\}^2 = \Sigma\, \epsilon^2 \tag{9}$$

where the summations are taken over all the sample points. We make two observations:

(1) If K is known, then solutions for A and B may be found easily and analytically. They are

$$A = \frac{\Sigma\, xy - B\, \Sigma\, ty}{\Sigma y^2} \tag{10}$$

and

$$B = \frac{\Sigma\, xy\, \Sigma\, ty - \Sigma\, tx\, \Sigma\, y^2}{(\Sigma\, ty)^2 - \Sigma t^2\, \Sigma y^2} \tag{11}$$

where

$$y = 1 - e^{-Kt}$$

and all summations are taken over the entire data set.

(2) If A and B are known, the equation (7) can be solved for K:

$$K = -\frac{1}{t} \ln \frac{A + Bt - x}{A} \quad . \tag{12}$$

Define a variable z, for each observation, to be

$$z = -\frac{1}{t} \ln \frac{A + Bt - x_o}{A} \quad . \tag{13}$$

A natural estimate for K given A and B would be

$$K = \bar{z} = \frac{1}{N} \Sigma\, z. \tag{14}$$

If the errors were all zero and the data fit the model exactly, then the variance of the z's would be zero. Thus the variance of z will be a measure of the goodness of fit of the model.

The scheme adopted for finding A, B, and K is as follows:

(1) Guess a value of K.

(2) Estimate A and B from equations (10) and (11) using the estimated value of K.

(3) Estimate K from equation (14) using the estimates of A and B.

(4) Repeat steps (2) and (3) until there are no more significant changes in the estimates.

When this method is applied to the entire set of data, it tends to converge to values of A and B with $(A + Bt - x)/A < 0$ for those points with $x > 115$ mm. This makes the computation of K by the scheme above impossible.

Three modifications of the fitting scheme were used and results for each are shown in Table IV.

Scheme 1. Only those points for which $x < 115$ were used.

Scheme 2. All the points were used; when $(A + Bt - x)/A < 0$ that point was not used in the estimate of K on that iteration. This method did not converge; rather it cycled with $(a - Bt - x)/A$ going negative on every fourth or fifth iteration for one or more of the points. The results shown in the table were picked from the cycle at random.

Scheme 3. All the data points were used to estimate A and B for given K; but then only those points for which $x < x_{crit}$ were used to find the next value of K. Results are shown for $x_{crit} = 115$ and 100 mm.

In schemes 1 and 3 the procedure converged after about 200 iterations, or less than 2 minutes of computer time. Some empirical testing was done to verify that values at which the procedure converged were independent of the starting estimate of K.

TABLE IV

RESULTS FOR DIFFERENT ESTIMATING SCHEMES

Scheme	A	B	K	Mean Square Error*	Mean Square Error for the Points with x < 100	Variance of z	Remarks
1	58.37	1.691	0.0608	0.192	0.124	2.9×10^{-6}	
2	41.39	2.140	0.0764	0.490	0.223	7.5×10^{-6}	
3a	41.13	2.145	0.0753	0.449	0.193	2.1×10^{-5}	< 115 mm for K
3b	40.21	2.164	0.0771	0.426	0.177	8.1×10^{-6}	< 100 mm for K

*Mean square error is defined as:

$$\text{m.s.e.} = \frac{1}{N} \Sigma(x_o - [A - A\, e^{-Kt} + Bt])^2$$

Schemes 2 and 3 gave results that were only marginally different, with 3b giving the best. Figure 7 lists the values of the coefficients A, B, and K and shows a comparison of the observed with the calculated values of x computed by scheme 3b. Also listed are values of the residuals, the sum of the residuals, and the sum of the squares of the residuals. Figure 8 presents a graphical comparison of the experimental and analytical data.

In section IVB, we give an interesting comparison of these results with those reported by Jaffe, Beauregard, and Amster.[7] Those authors performed experiments which, in every way but one, were identical to ours: in lieu of propellant they used a Lucite acceptor and their results, also shown in Fig. 8, are essentially identical to ours.

3. Results

Because of the excellent fit of the data with the computed coefficients we use the following equations to represent the attenuating shock in the x-t and $\dot{x}$-t planes for $x < 153$ mm:

$$x = 40.21(1 - 3^{-0.0771t}) + 2.164t,$$

$$\dot{x} = U = 3.1002 \exp(-0.0771t) + 2.164.$$

Later we will use the second of these equations to compute the shock pressure.

A= 40.2050	B= 2.1640	K= 0.0771	
T[I]	OBS.X[I]	EST.X[I]	RESID.
1.30000	6.60400	6.64852	-0.04452
1.35000	6.75600	6.89669	-0.14069
1.33000	6.85800	6.79749	0.06051
1.40000	6.88300	7.14433	-0.26133
2.60000	13.10600	12.93118	0.17482
2.60000	13.18300	12.93118	0.25182
2.55000	13.13200	12.69587	0.43613
2.70000	13.15700	13.40033	-0.24333
3.95000	19.05000	19.10561	-0.05561
3.95000	18.92300	19.10561	-0.18261
5.40000	25.40000	25.38003	0.01997
5.45000	25.40000	25.59026	-0.19026
5.35000	25.40000	25.16941	0.23059
5.40000	25.40000	25.38003	0.01997
6.90000	31.75000	31.52204	0.22796
7.00000	31.75000	31.91986	-0.16986
6.90000	31.75000	31.52204	0.22796
7.00000	31.75000	31.91986	-0.16986
8.48000	38.10000	37.65019	0.44981
8.55000	38.10000	37.91422	0.18578
8.53000	38.10000	37.83885	0.26115
8.60000	38.10000	38.10244	-0.00244
10.03000	43.96700	43.35977	0.60723
10.03000	44.39900	43.35977	1.03923
10.28000	44.60200	44.25499	0.34701
10.33000	44.95800	44.43322	0.52478
12.10000	50.80000	50.57629	0.22371
12.00000	50.80000	50.23747	0.56253
12.05000	50.80000	50.40700	0.39300
12.00000	50.80000	50.23747	0.56253
16.15000	63.50000	63.58258	-0.08258
16.05000	63.50000	63.27660	0.22340
16.23000	63.50000	63.82687	-0.32687
16.15000	63.50000	63.58258	-0.08258
20.60000	76.20000	76.57368	-0.37368
20.50000	76.20000	76.29372	-0.09372
20.60000	76.20000	76.57368	-0.37368
25.25000	87.50300	89.11029	-1.60729
24.98000	87.50300	88.40533	-0.90233
25.35000	89.15400	89.37075	-0.21675
25.65000	90.29700	90.15012	0.14688
29.15000	98.67900	99.03974	-0.36074
30.28000	101.44800	101.83941	-0.39141
31.90000	102.61600	105.80213	-3.18613
35.35000	115.21400	114.07025	1.14375
35.60000	115.41800	114.66152	0.75648
40.80000	127.40600	126.76728	0.63872
41.30000	127.68600	127.91468	-0.22868
46.25000	140.25900	139.15437	1.10463
46.85000	140.84300	140.50412	0.33888
52.50000	153.03500	153.11369	-0.07869
SUM AND SUM SQRS		1.3936	21.7536

FIG. 7 OBSERVED vs ANALYTICAL VALUES OF x

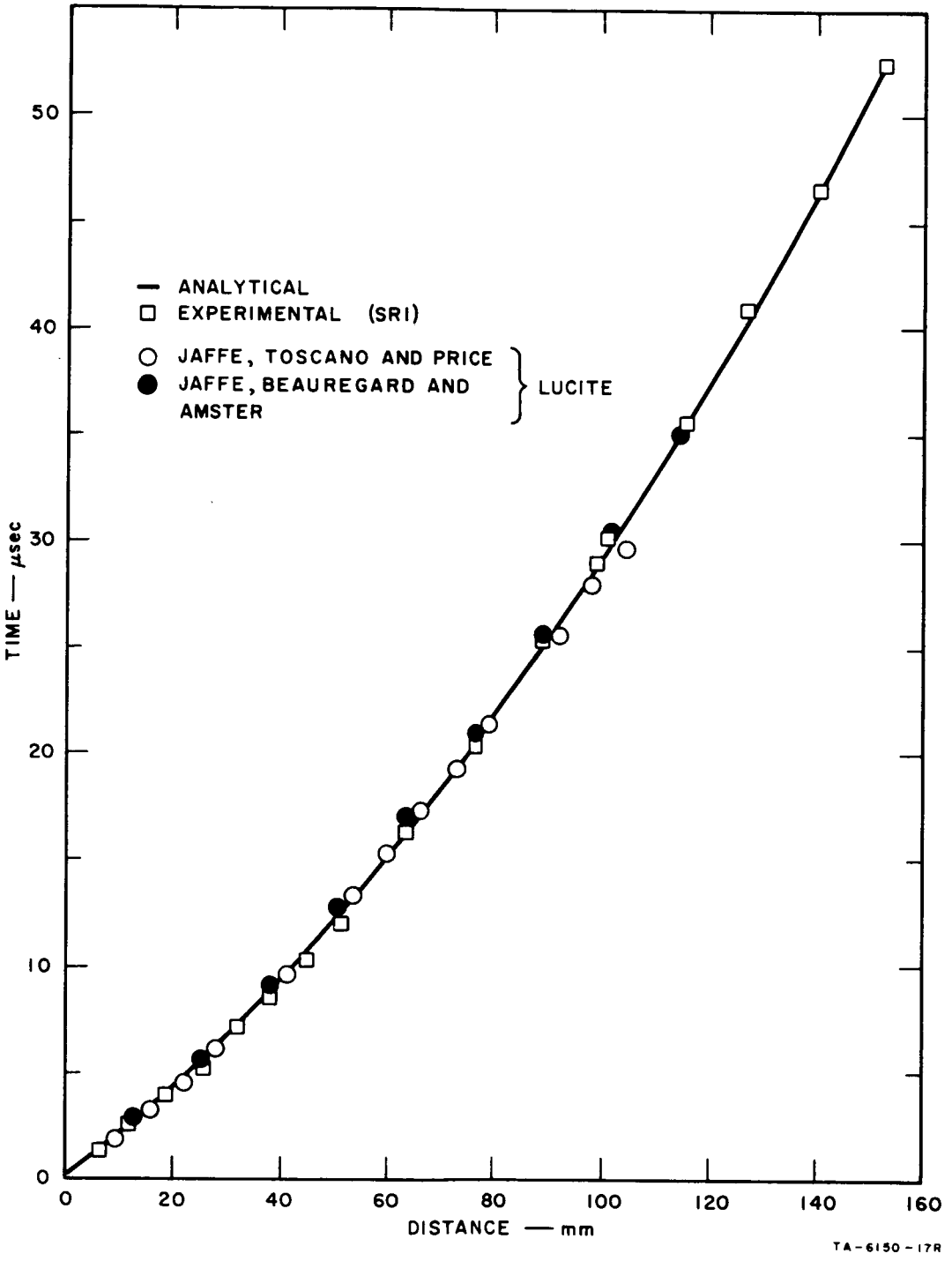

FIG. 8 EXPERIMENTAL vs ANALYTICAL VALUES

C. Propellant Sonic Velocity

The lower limit to the shock velocity is the longitudinal sound velocity; this value also serves as an important parameter in "anchoring" the Hugoniot. Consequently, we performed experiments to measure the speed of sound in PBAN-170 using the method described by Gottleman and Evans.[3] Briefly, the experiment consisted in imposing a square wave upon one end of a long sample and measuring the transit time to the other end. The transit time t varies linearly with sample thickness x, but because of edge and end effects the line does not pass through the origin. The slope of the line dx/dt is nevertheless a precise measure of the sound velocity. The experimental results are summarized in Table V and Fig. 9. The figure shows the linearity of the fit. From a least squares fit of the data the speed of sound was found to be 2.13_2 mm/μsec. This we believe to be in good agreement with the value of 2.16_4 mm/μsec obtained from the attenuation studies and reported in the preceding paragraph.

TABLE V

TRANSIT TIME OF SOUND WAVE IN PBAN-170

Sample Number	Thickness mm	Transit Time μsec
1	2.54	1.19 ± 0.1
2	5.08	2.47 ± 0.1
3	7.49	3.27 ± 0.1
4	10.16	4.41 ± 0.1
5	12.6	5.78 ± 0.2
6	15.1	6.75 ± 0.2
7	17.8	8.11 ± 0.2

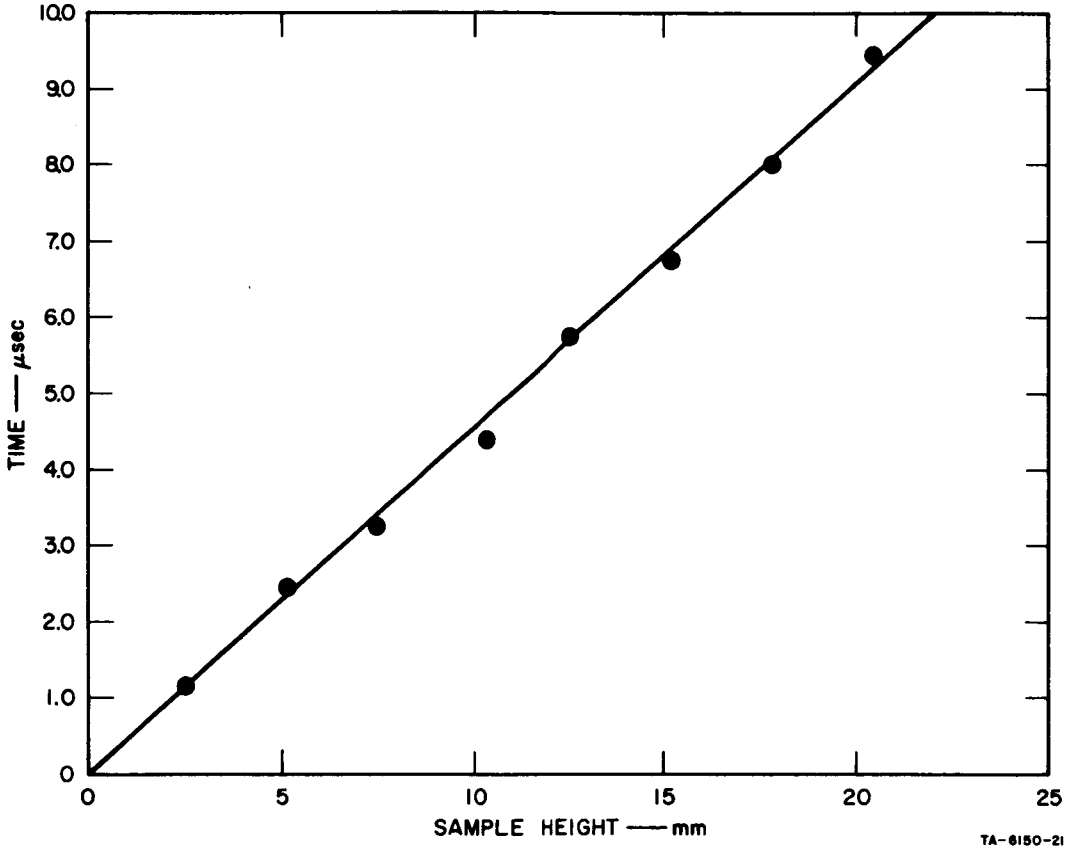

FIG. 9 SONIC VELOCITY IN PBAN-170

D. Equation of State

1. Introductory Discussion

Classically, the Hugoniot of a material is the graphical or analytical representation in the P-ρ plane of the locus of all states in that plane that can be reached from an initial state (P_o, ρ_o, E_o) by shock compression, where P, ρ and E are the pressure, density, and internal energy. Unlike adiabatic compression, which is ideally a reversible process, shock compression is not reversible. The shock compression conservation equations that relate p and ρ are

$$P - P_o = \rho_o U_s U_p, \tag{15}$$

$$\rho_o/\rho = (U_s - U_p)/U_s, \tag{16}$$

where U_s and U_p are the shock velocity and particle velocity, respectively. The Hugoniot is constructed from values of P and ρ_o/ρ. Since P_o and ρ_o are generally known, the Hugoniot is determined when the relation between U_s and U_p is experimentally generated.

We investigated several experimental methods to obtain U_s and U_p for PBAN-170 (see, for example, Rice et al.[9] and Duvall[10]), but only those three which we actually used will be detailed. At the outset, it was apparent that at least two methods would be necessary to cover the desired pressure range: 0 to 100 kbar.

The methods which were applicable at high pressure, such as the contact explosive method, do not give reliable data at pressures below 15 to 20 kbar. The low pressure methods such as the oblque shock technique cannot be designed to give pressures greater than about 20 kbar in plastic-like materials.

2. Low Pressure Regime

a. Oblique Shock Method

The oblique shock method developed by Fowles[11] is particularly applicable to studying the low pressure region (0-20 kbar), within which any elastic-plastic transition might be expected to occur. For example, this technique was used successfully by Evans and Schmidt[12] to study Plexiglas in this same pressure region.

Figure 10 depicts the experimental arrangement we used. A shock wave which decays with distance x is induced in the propellant wedge by the detonating sheet explosive. Under these conditions the shock velocity at any point is given by

$$U_s = U_D \sin \theta = U_a \sin \gamma, \tag{17}$$

where U_D is the detonation velocity in the explosive sheet, U_a is the velocity with which the shock intersects a plane parallel to the wedge surface AF such as CE, and θ is the angle between AF and the tangent to the advancing wave. From geometric considerations, it is seen that

$$\cot \theta = \cot \alpha + U_D/U_a \sin \alpha. \tag{18}$$

Thus from a measurement of α, U_D, and U_a, we can calculate U_s using equations (17) and (18). The free surface velocity, U_{fs}, which is related to U_p by the free surface approximation, $U_p = U_{fs}/2$, can be determined from the experiment.

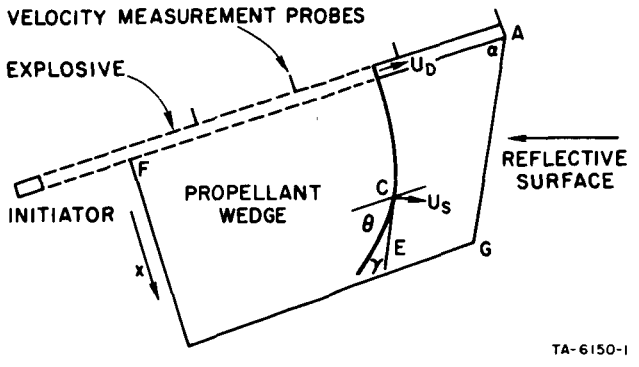

FIG. 10 TEST ARRANGEMENT FOR OBTAINING LOW PRESSURE HUGONIOT BY OBLIQUE SHOCK METHOD

The experiment consists of viewing the lighted surface of the wedge with a streak camera. Point source lighting and a grid image are provided by an exploding argon candle fitted with a transparent grid. The lines of the image are perpendicular to the plane of the sketch in Fig. 10. The arrival of the shock wave at the free surface causes the image of the grid lines to shift. From the extent of the shift the free surface velocities are obtained; the rate of the shift gives U_a. The advantage of a continuous recording of the free-surface motion is that it gives in a single experiment a range of U_s-U_p data and shows if there is an elastic wave preceding the shock.

We were able to solve some of the problems associated with applying this experimental method to large wedges of propellant. These included line initiation of the sheet explosive, propellant mold releasing agents, smooth-reflective surfaces, and uncertainty in wedge angle α. With an error analysis we were able to show that the uncertainty in α would not

be the limiting error. However, for reasons not fully understood our film records are cloaked in the critical region by what appears to be smoke--though every precaution was taken to eliminate these problems. Because of time limitations this approach was finally abandoned. Even though we were not able to obtain useful U_s-U_p data, we could conclude from these experiments that there was evidence of no elastic precursor wave.

b. Aquarium Method

Since the oblique shock method was unsuccessful, we investigated the "aquarium" or impedance mismatch method.[13,14] In this experiment the shock is followed as it travels from the sample into a material of known equation of state, i.e., one for which the U_s-U_p relation is known. This material is usually water because of its well defined equation of state, thus the name "aquarium." Equation (19) is then used to calculate the particle velocity in the sample:[7,13]

$$(U_p)_t = (U_p)_{H_2O} \frac{(\rho_o U_s)_{H_2O} + (\rho_o U_s)_t}{2(\rho_o U_s)_t} \qquad (19)$$

where the subscript t stands for the material being tested. This equation requires that the U_s-U_p relation be known for both materials in the pressure region about the interface.

Figure 11 is a schematic diagram of the test arrangement. A typical streak shadowgraph from an aquarium experiment is shown in Fig. 12. Line A-B represents the shock in the Plexiglas. The time from B to C is the transit time in the opaque propellant. Line C-D is the shock transmitted into the water. Because U_s-U_p data are also available for Lucite equation (19) can also be applied to the attenuator-propellant interface.

3. High Pressure Regime

The contact explosive method was employed in the high pressure region ($>$ 20 kbar). In these experiments small thin cylinders ($\sim$ 2.5 and $\sim$ 5.0 mm) were placed on a specimen plate of aluminum or brass and a plane shock wave imposed on them. Figure 13 shows a schematic diagram of the test arrangement. By varying the composition of the explosive donor (Comp B or Baratol) and the thickness and composition of the attenuators, a plane shock wave of various strengths was generated (see, for example, Coleburn[15]). The transit times through the thin propellant samples and thus the average shock velocity were measured by viewing, with a streak camera, the lighted surfaces of the samples which had been made reflective by an aluminized Mylar strip. The time of disappearance of the images from the free surface mirrors above some of the samples and on the specimen plate was used to compute the free surface velocity of the propellant and specimen plate. The particle velocity in the propellant was calculated using both the free surface approximation and the impedance matching method (see Rice et al.[9] for a discussion and analysis of both methods). A typical trace is shown in Fig. 14. Point A is the arrival of the shock at the specimen plate surface. The shock arrives at the propellant surfaces at B and B'. A-C is the plate free surface time, and B-D and B'-D' are the free surface times of the samples.

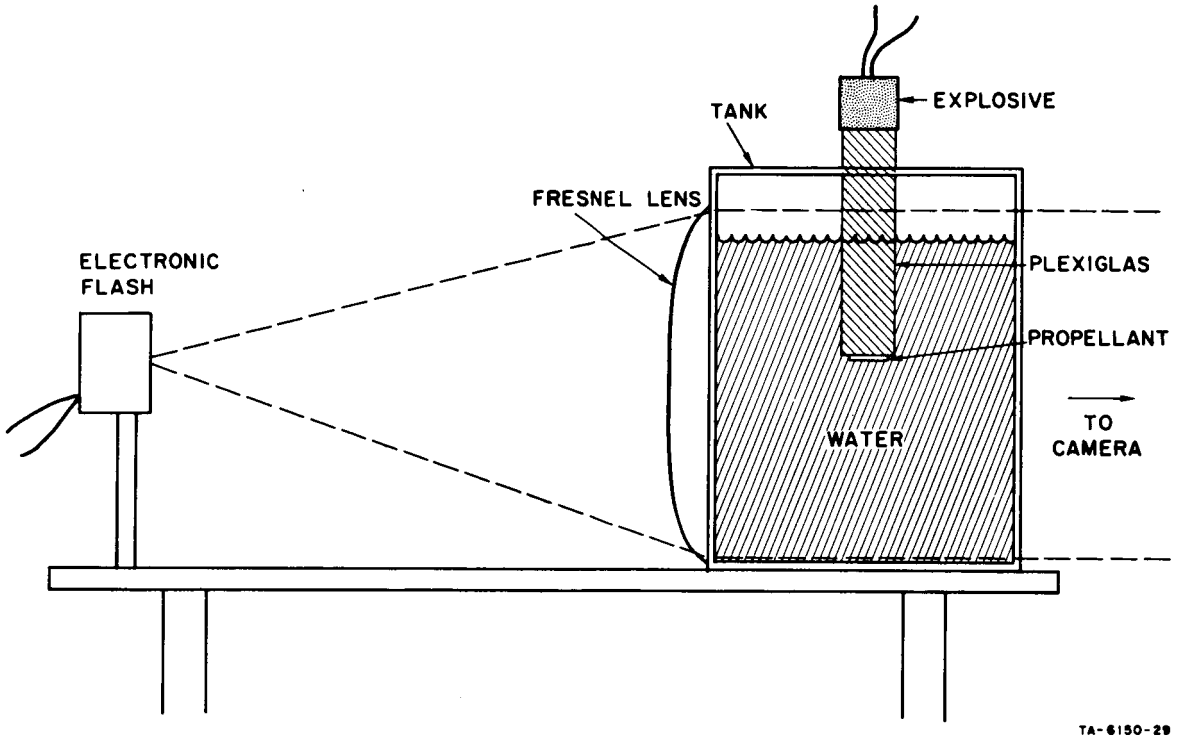

FIG. 11 TEST ARRANGEMENT FOR EQUATION OF STATE MEASUREMENTS BY AQUARIUM METHOD

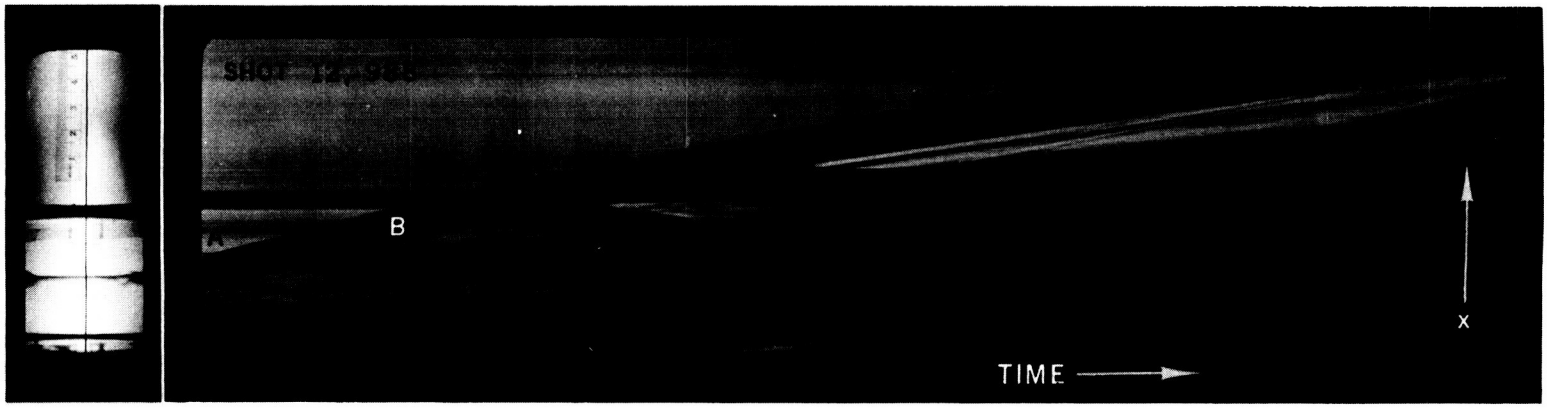

1 μsec

LINE A-B: SHOCK IN PLEXIGLAS
LINE B-C: SHOCK IN OPAQUE PROPELLANT
LINE C-D: SHOCK IN WATER

TA-6150-35

FIG. 12 PHOTOGRAPHIC RECORD FROM AQUARIUM METHOD

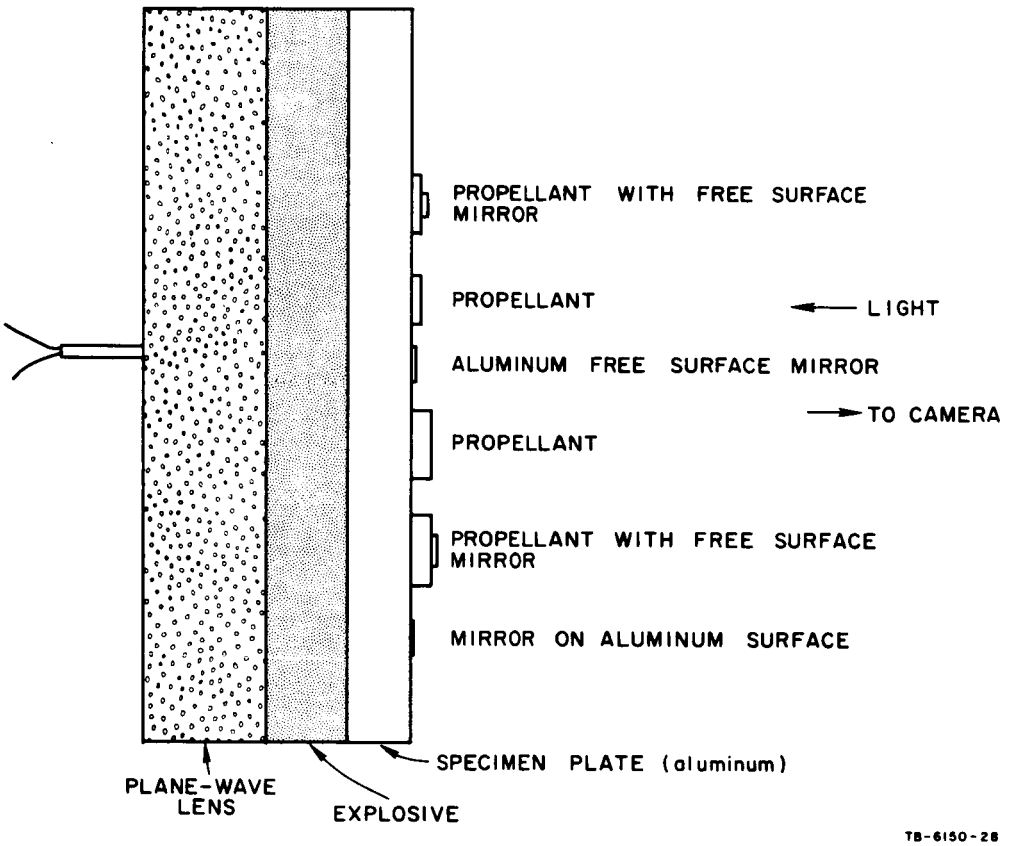

FIG. 13 TEST ARRANGEMENT FOR EQUATION OF STATE MEASUREMENTS BY CONTACT EXPLOSIVE METHOD

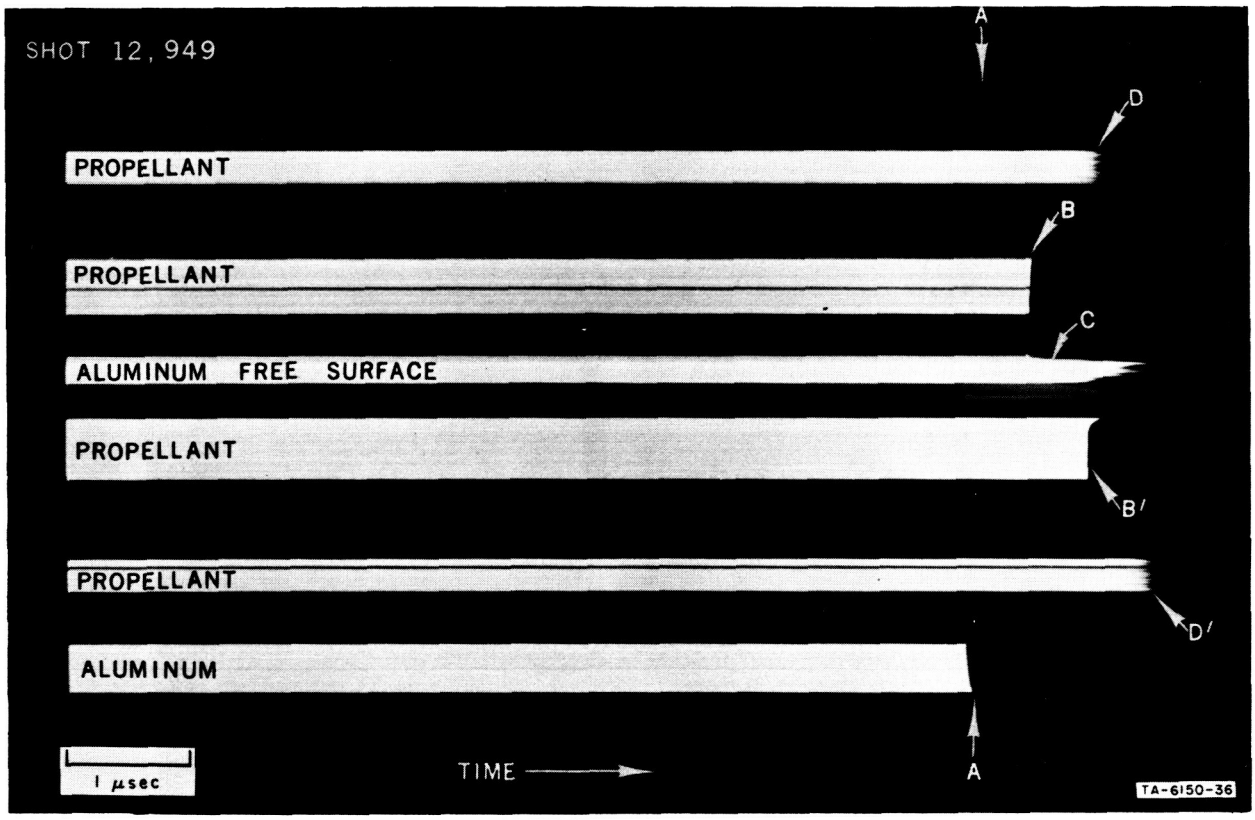

FIG. 14 PHOTOGRAPHIC RECORD FROM CONTACT EXPLOSIVE EXPERIMENT

4. Experimental Equipment

All photographic data were collected with a Beckman and Whitley smear camera Model 770. This camera has a maximum writing speed of 10.17 mm/μsec at 3000 cps and records for 20 μsec at this speed. We used 70 mm Kodak Tri X film which was developed in HC110 at 68°F for 6.5 minutes. A slit of 0.05 mm was used in the contact explosive experiments while one of 0.10 mm was used for the low pressure experiments. Lighting for the contact explosive and oblique shock experiments was provided by an exploding argon candle. This candle consists of an open-ended wooden box 13 x 18 x 30 cm whose inside is aluminized. The box is closed at one end by an explosive pad and the other by a frosted glass plate. The box is filled with argon gas which becomes exceptionally brilliant when an explosive shock is driven into it. The electronic flash used in the aquarium experiments was a Spiralite flash head. This flash unit was operated on a 115 AC circuit and flashed by the smear camera triggering unit.

5. Experimental Results

The equation of state data which we obtained for PBAN-170 are summarized in Table VI. The methods by which the data were obtained are also listed. Many investigators have found that the relation between U_s and U_p is a linear one.[9] Figure 15 is a plot of our data with a best least squares fit shown by the straight line:

$$U_s = 2.22 + 1.71\ U_p. \tag{20}$$

The intercept at 2.22 mm/μsec is only 4.2% higher than the measured sound velocity of 2.13 mm/μsec. Both the sound velocity and the shock velocity

TABLE VI

EQUATION OF STATE DATA

Shot No.*	Temp. °K	Sample Thickness mm	U_s mm/μsec	Up mm/μsec	P kbar	ρ_o/ρ	Type of Analysis**
12,949	291	2.56_5	4.72_5	1.46_4	116.9	0.690	1
		5.08	5.00_4	1.67_1	141.3	0.666	1
		2.56_5	4.72_5	1.46_8	117.2	0.689	2
		5.08	5.00_4	1.44_5	122.0	0.711	2
12,968	289	5.15	2.99	.244	12.3	0.918	1
		2.60	3.11	.231	12.2	0.926	1
		5.15	2.99	.315	16.5	0.895	2
		2.60	3.11	.317	16.0	0.898	2
12,974	291	2.60	4.31_6	1.17_1	85.5	0.729	1
		5.00	4.48_6	1.24_9	94.6	0.722	1
		2.00	4.31_6	1.35_6	98.8	0.686	2
		5.00	4.48_6	1.34_2	101.3	0.701	2
12,975	295	2.60	3.56_3	1.03_6	62.3	0.709	1
		5.00	3.84_4	1.04_3	67.8	0.729	1
12,988	293	4.95	3.39	0.609	34.9	0.820	3
		4.95	3.39	0.733	42.0	0.784	4
13,002	294	4.97	2.14	0.038	1.40	0.982	3
		4.97	2.14	0.124	4.48	0.942	4
13,003	294	4.97	2.23	0.147	5.55	0.934	3
		4.97	2.23	0.248	9.34	0.889	4

*Shot Nos. 12,949-12,975 were contact explosive experiments.
Shot Nos. 12,988-13,003 were aquarium experiments.

**Types of analysis: (1) measured free surface velocity, (2) impedance matching, (3) aquarium-water equation of state,[14] (4) aquarium-Plexiglas equation of state.[12,15]

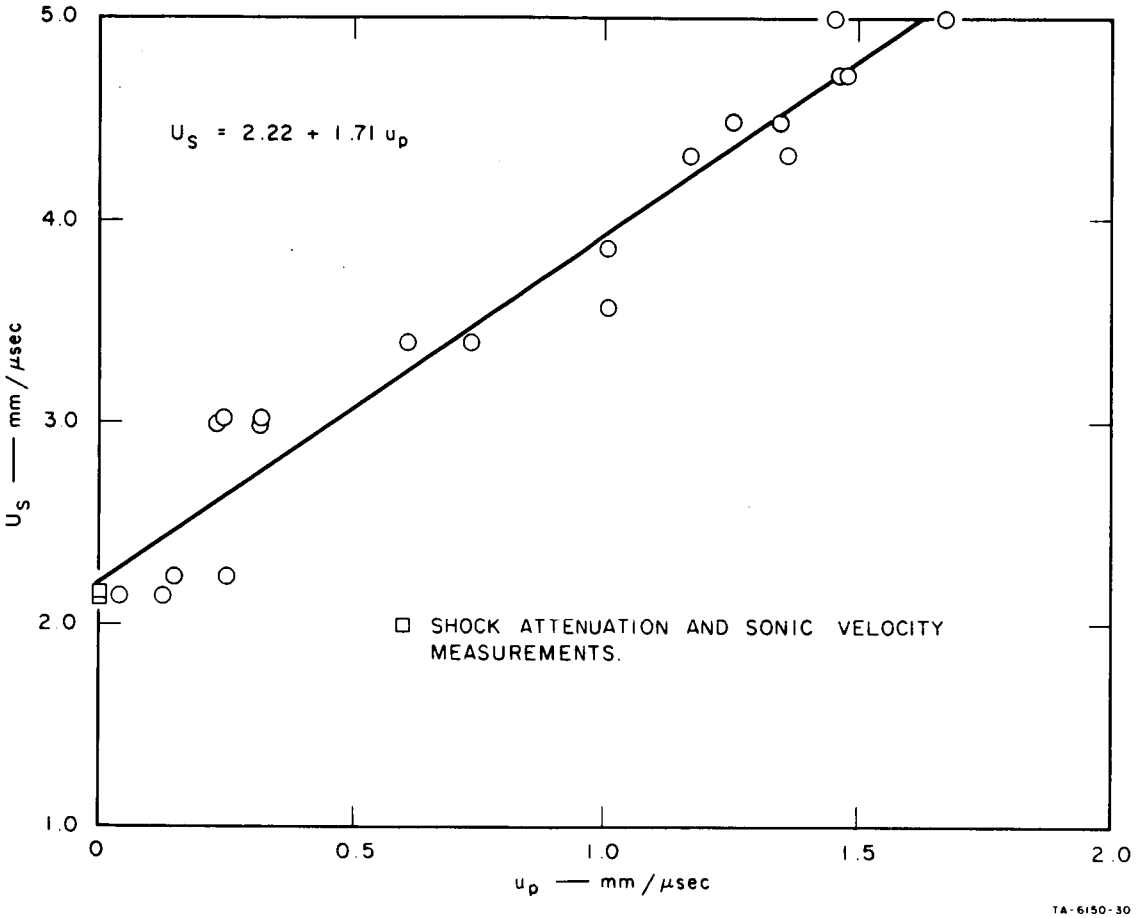

FIG. 15 SHOCK VELOCITY (U_s) vs PARTICLE VELOCITY (U_p)

at infinite thickness (2.16 mm/μsec) obtained from the shock attenuation experiments are shown in Fig. 15. Equation (20) with equations (15) and (16) define a Hugoniot for PBAN-170. Figure 16 shows the Hugoniot in the P-U_p plane. The points were computed using equation (15) and the experimental results. The line shown is that of equation (20), transformed to the P-U_p plane using equation (15). Classically, the Hugoniot is represented in the P-ρ plane by plotting the pressure versus the dynamic compressibility, i.e., density ratio, ρ_o/ρ. Such a representation is shown in Fig. 17.

Our data do not show a break in the pressure-density curve that would correspond to a plastic-elastic transition, but they do seem to fit a smooth curve in the expected region. However, this transition may occur at a still lower pressure (< 1 kbar) where we would not have detected it.

Using the data for the equation of state and the shock attenuation for PBAN-170, a pressure-shock travel distance curve was constructed. This is shown in Fig. 18 for tetryl-loaded PBAN-170.

E. Air Blast Measurements

1. The Equivalence Factor

One of the objectives of this program was to determine what fraction of a sample propellant in contact with a detonating explosive charge will contribute to the total blast wave in air. This contribution is most readily expressed in terms of an equivalence factor f; the basic assumption is that

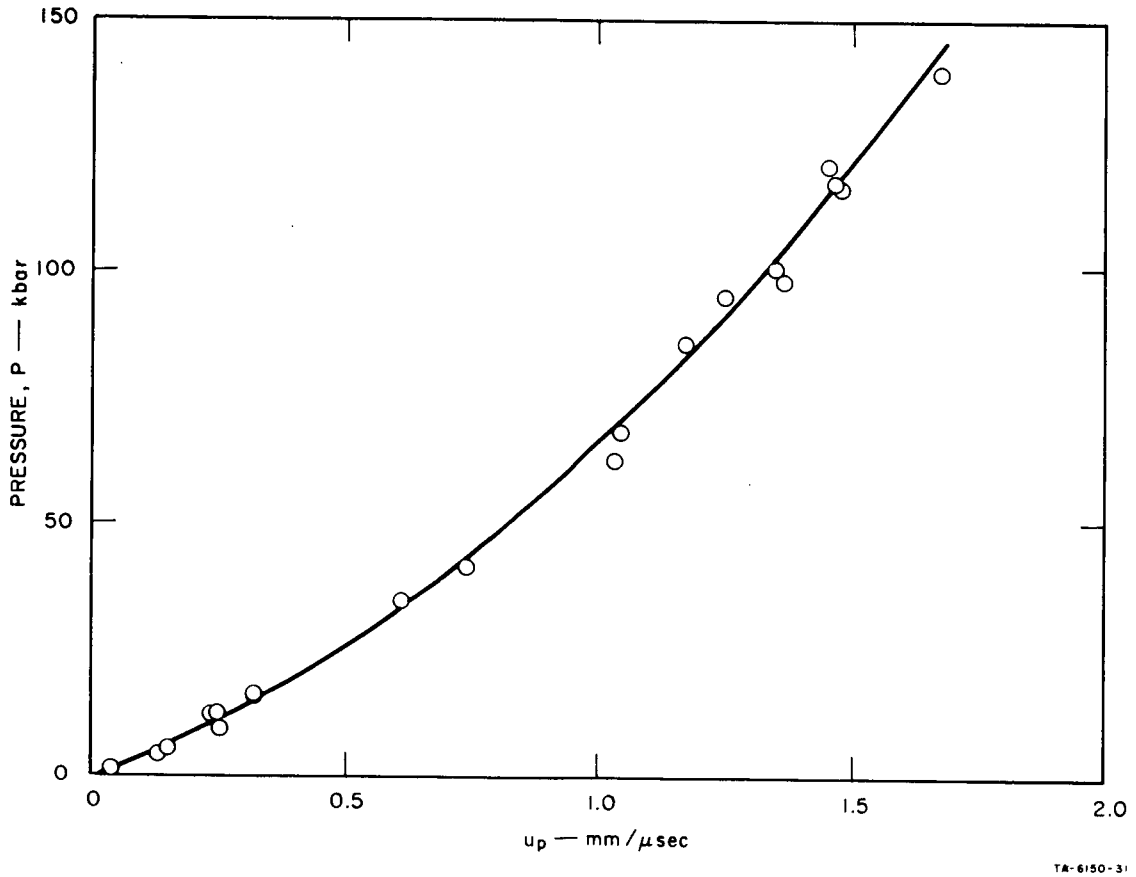

FIG. 16 HUGONIOT RELATION FOR PBAN-170

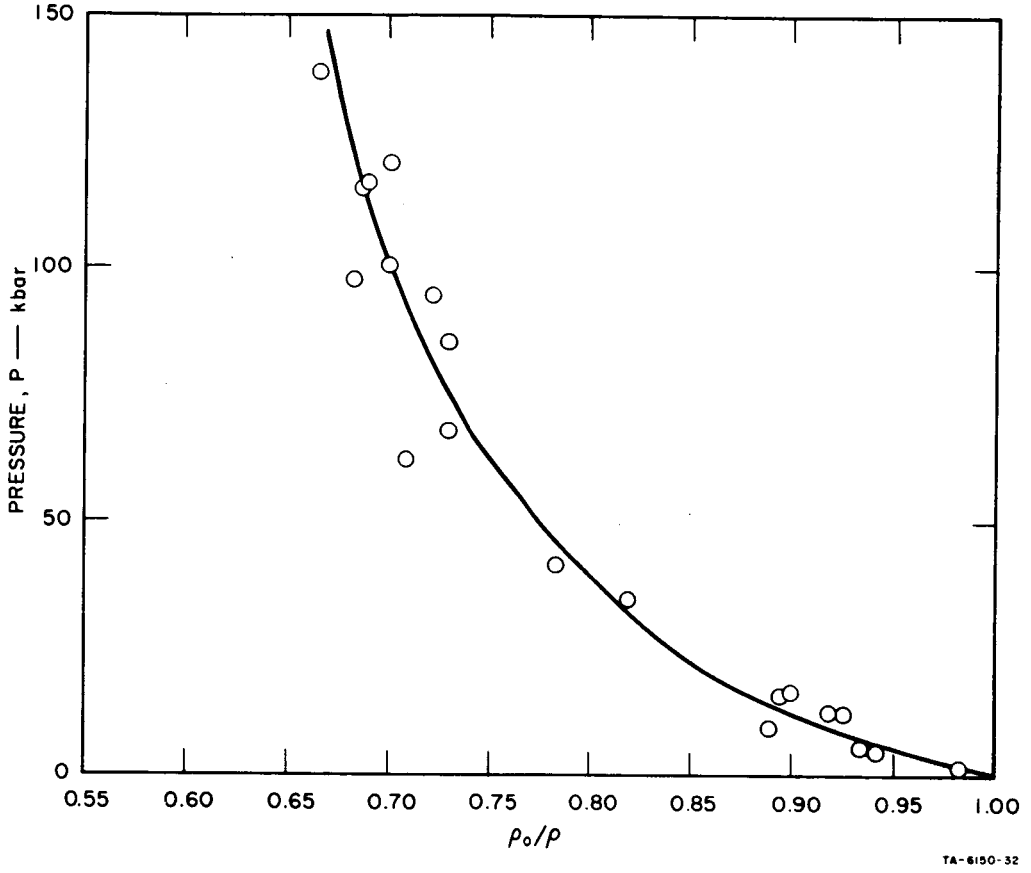

FIG. 17 DYNAMIC COMPRESSIBILITY RELATION FOR PBAN-170

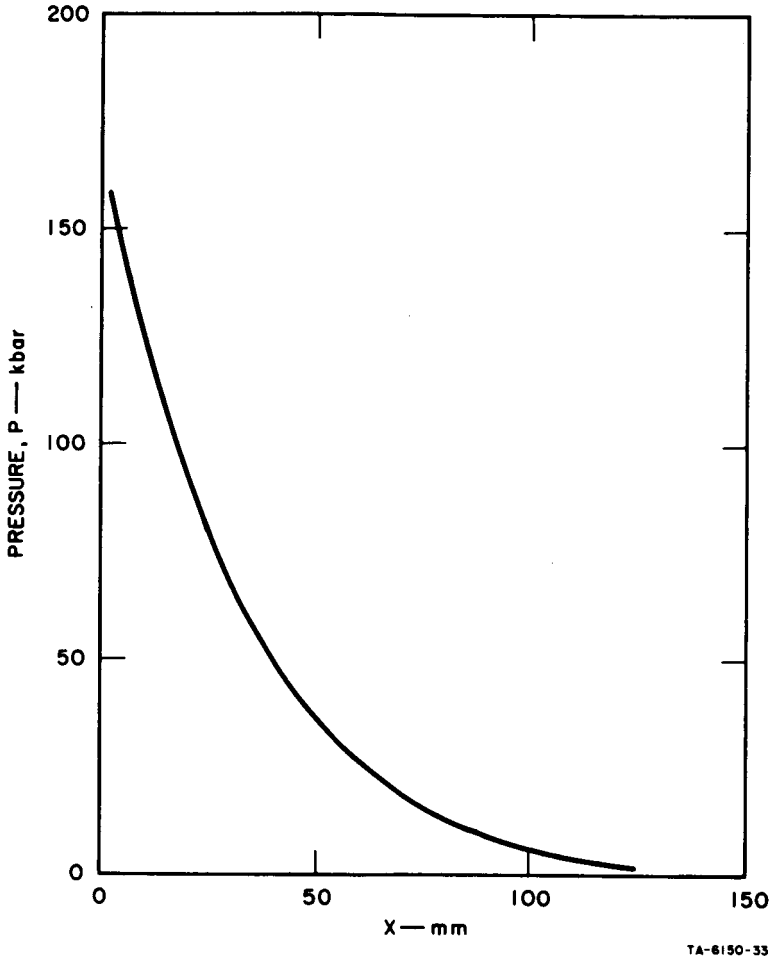

FIG. 18 PRESSURE vs TRANSIT DISTANCE FOR TETRYL-LOADED PBAN-170

a mass W of explosive plus propellant produces essentially the same blast wave as would a mass fW of the same explosive alone. A knowledge of the ratio of the (specific) energy of explosion of the explosive to that of the propellant then permits a reasonable estimate of the mass of propellant that actually contributed to the blast wave.

A standard technique for determining f depends on the well-established fact that, to a good approximation, the peak overpressure ratio (or, equivalently, the shock Mach number) for most secondary explosives detonated in air under near-standard conditions is contingent only on the parameter $rE^{-1/3}$, where r is the distance from the center of the charge and E is the total energy released by the explosion. At great distances, the peak overpressure ratio is affected only slightly by the details of the charge configuration and the exact rate of energy release. Accordingly, if two explosions with energy release E_1 and E_2 produce a given peak overpressure ratio at distances r_1 and r_2, respectively, we must have

$$r_1 E_1^{-1/3} = r_2 E_2^{-1/3}.$$

For a given explosive, E is proportional to W, the mass of the charge, and we have

$$W_2 = W_1 (r_2/r_1)^3.$$

In the case at hand, W_1 is the mass of the explosive alone, and $W_2 = fW_1$ is the equivalent mass corresponding to the blast produced by the explosive plus propellant. We then have

$$f = (r_2/r_1)^3,$$

where r_1 is the distance at which detonation of the explosive alone produces a given peak overpressure and r_2 is the distance at which the explosive plus propellant produces the same overpressure. A measure of the extent to which the basic assumptions as to the effect of charge configuration and energy release rate are valid is provided by the dependence of the value of f on the peak overpressure used to determine r_1 and r_2; a further experimental check is to compare two explosive charges of different size (without propellant) and to note the agreement between f and the known ratio of charge weights.

Evidently, the application of this method requires the determination of the radius as a function of peak overpressure for each explosion; if several explosions are to be compared, the corresponding ranges of overpressures must have significant overlap.

2. Pressure Gauge Studies

Peak pressure-distance relations can be obtained directly from measurements of the shock velocity. Very high frequency piezoelectric gauges, such as the Kistler or ARC units conjoined with oscilloscopes, give pressure-time data directly. Barium titanate piezoelectric gauges, used similarly, will give only the arrival time. When several such gauges are located accurately along a radius from the shock source, differentiation of the collected data yields velocity and, from the equation of state for air, the desired peak pressures.

Each method has its advantages. The high frequency gauges give directly the pressure-time history and with it both peak pressure and impulse at a given position. Even the best gauges of this class, however, suffer from inaccuracy and, because of the complications of ancillary electronic equipment, unreliability. They are also expensive (up to $1000 per channel).

The time-of-arrival gauges are simple and reliable; they cost about two or three dollars each. They do not give impulse data and peak pressure are obtained only upon differentiation as noted above, but the equation of state for air is known with considerable accuracy and gauge coordinates can be precisely established. Because of the merits and drawbacks of each type of measurements, we decided to use primarily an array of barium titanate gauges in conjunction with a pair of high frequency gauges. For this reason we calibrated two ARC and two Kistler gauges so that we might use the best of these.

a. Calibration of Gauges

Two Kistler and two ARC gauges were calibrated by the method described by Cole.[16] The four gauges were mounted on a single cylinder in essentially equivalent positions. Then the cylinder was slowly pressurized by means of a precision dead-weight tester to precisely measured levels of up to 100 psi. The pressure was abruptly lowered to 0 psi with a quick-acting release valve, and the gauge outputs were recorded on oscilloscopes. The procedure was simple and reliable and the results were obtained quickly. To reduce the possibility of systematic errors, tests were run at every tenth-psi interval from 0 to 100, then back down to zero, and finally from zero to 100 again (e.g., 0, 10, 20, ..., 100, 90, ..., 0, 10, ...,100). The results of the tests are given in Table VII and in Figs. 19 and 20. The gauges with their associated cables, preamplifiers (for the Kistlers), connectors, etc., were stored for use in the air blast measurements as originally connected for their calibration.

TABLE VII

PRESSURE GAUGE CALIBRATION DATA*

Pressure psi	Deflection, volts											
	Kistler Gauge 1			Kistler Gauge 2			ARC Gauge 1			ARC Gauge 2		
	a	b	c	a	b	c	a	b	c	a	b	c
10	0.67$_5$	0.67$_5$	0.84	0.68$_0$	0.68$_0$	0.82	1.04$_5$	1.07$_5$	1.25	1.075	1.04$_5$	1.25
20	1.16$_5$	1.17$_5$	1.18$_5$	1.15	1.185	1.20	1.77	1.84$_5$	1.84	1.75	1.82$_5$	1.82$_5$
30	1.67$_5$	1.66$_5$	1.76$_5$	1.66$_5$	1.69	1.745	2.61	2.60	2.76	2.63	2.60	2.69
40	2.24	2.21	2.25	2.22	2.22	2.23	3.50	3.49	3.50	3.30	3.47	3.44
50	2.67	2.65	2.72	2.58	2.66	2.68	4.20	4.30	4.41	4.20	4.30	4.36
60	3.26	3.16	3.38	3.23	3.20	3.30	5.14	5.20	5.32	5.18	5.22	5.26
70	3.90	3.78	3.90	3.90	3.80	3.86	6.14	6.22	6.24	6.10	6.10	6.18
80	4.36	4.26	4.44	4.24	4.30	4.22	6.82	6.80	7.0	6.82	6.74	6.98
90	4.74	4.72	4.90	4.72	4.70	4.86	7.55	7.55	8.00	7.35	7.05	7.95
100	5.40	5.44	5.6	5.20	5.24	5.32	8.50	8.50	8.75	8.30	8.50	8.45

*a = order of testing 10, 20, ..., 100 psi; b = order of testing 100, 90, ..., 10 psi; c = same as "a" but performed after "b".

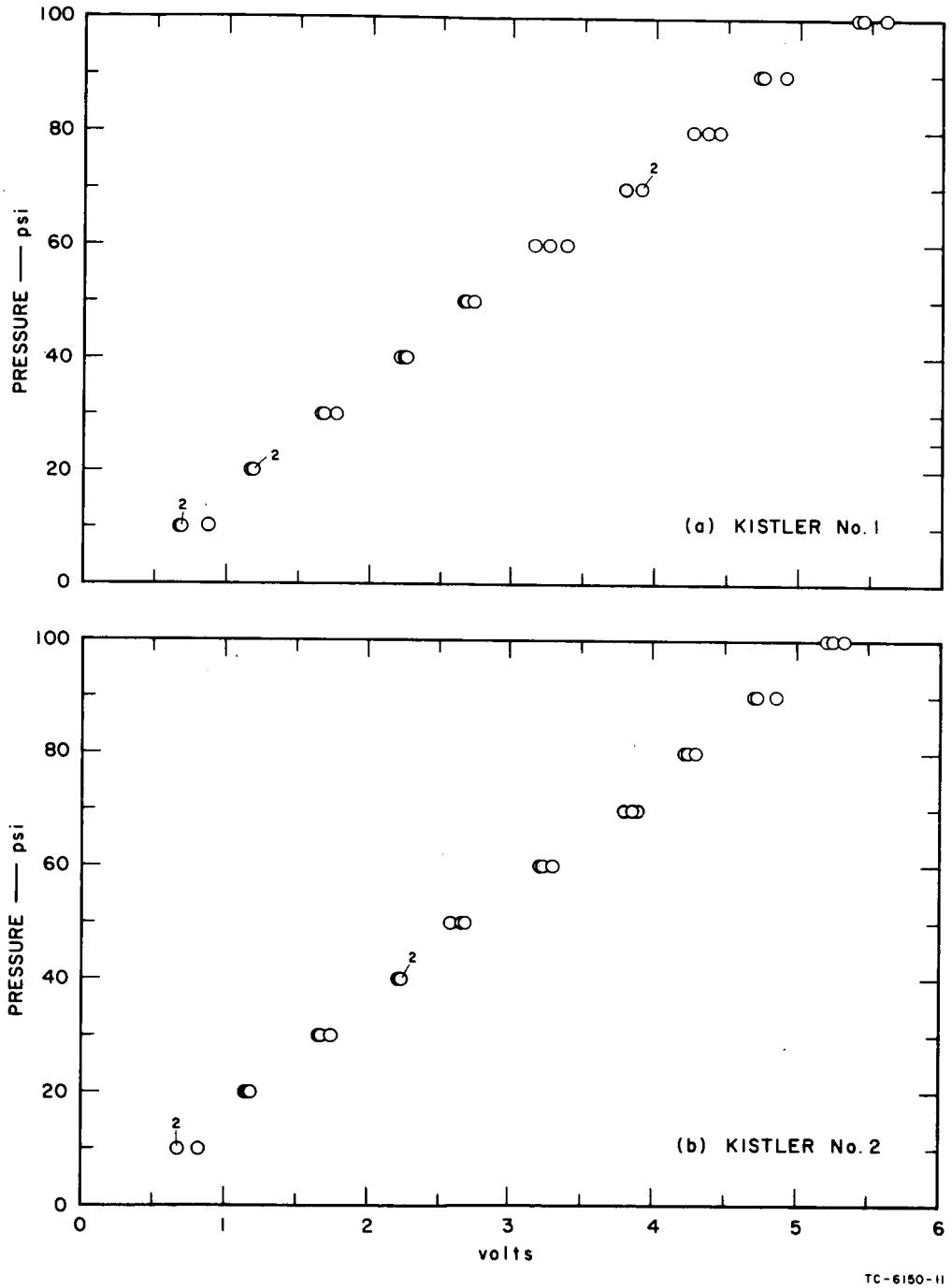

FIG. 19 KISTLER GAUGE CALIBRATIONS

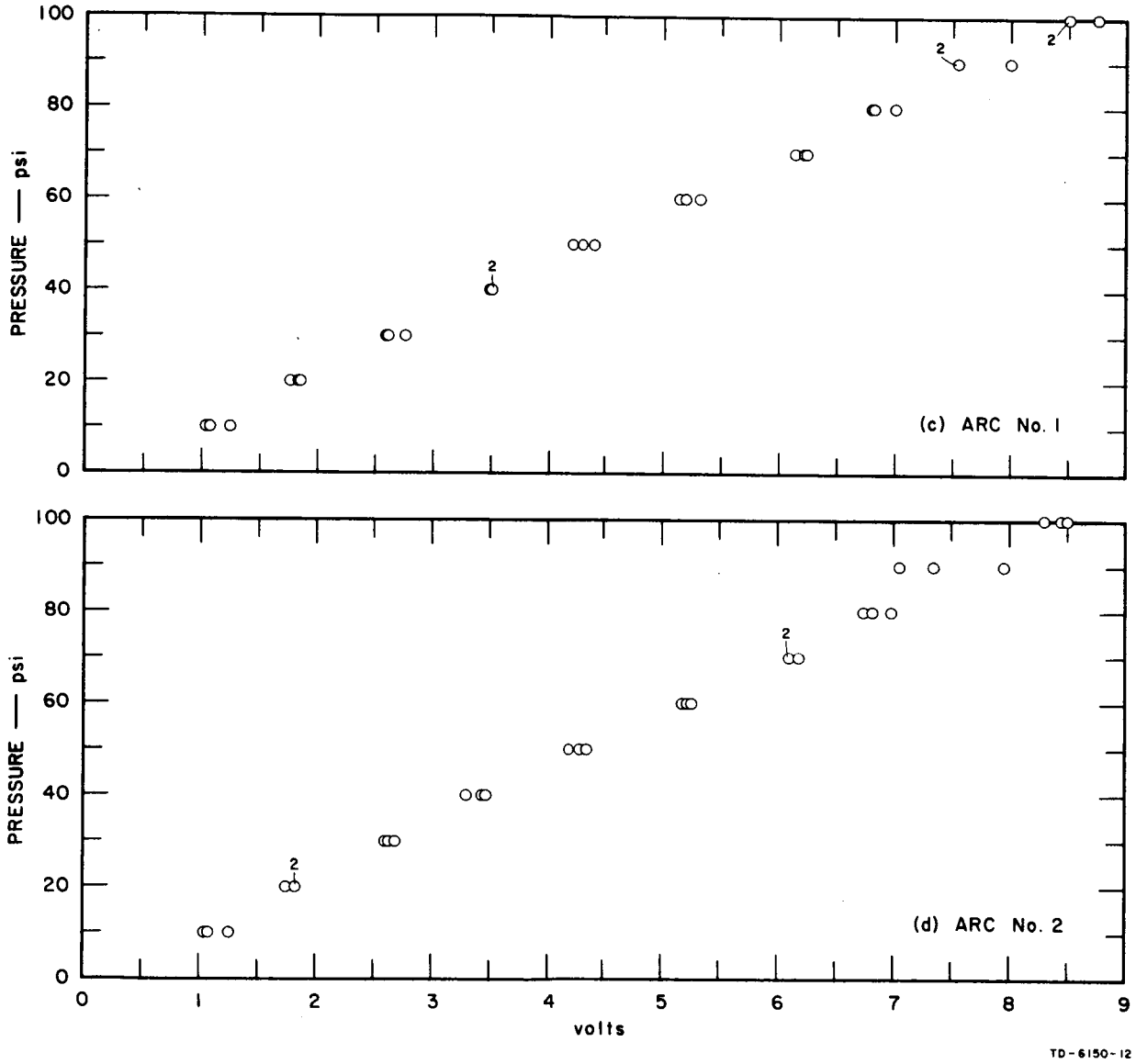

FIG. 20 ARC GAUGE CALIBRATIONS

b. Gauge Mount

The ARC gauge is supplied mounted in a "needle-nosed" support that is suitable for air blast measurements over a pressure range greater than that over which we will operate. For the Kistlers, on the other hand, suitable mounts are required. These are best described with the aid of the following sketch:

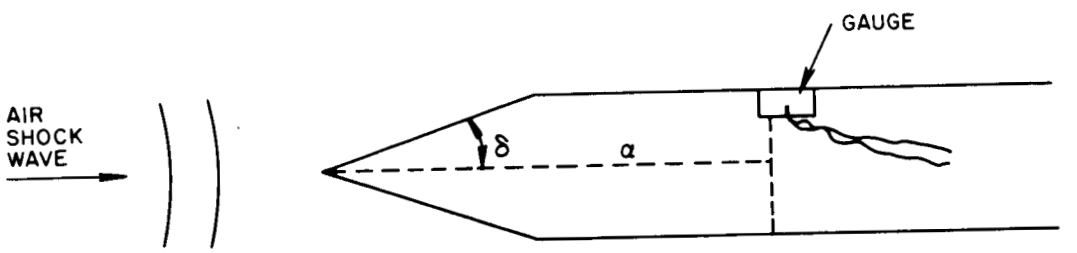

For the gauge response to be independent of the angle δ and to record the true air pressure, it is required that

$$\cot \delta \gg (M^2 - 1)^{\frac{1}{2}}$$

where

$$M = M_s - \left[\frac{(\gamma - 1)M_s^2 + 2}{2\gamma M_s^2 - (\gamma + 1)} \right]^{\frac{1}{2}}$$

and M_s is the shock Mach number. For air, $\gamma = 1.4$, and

$$M = M_s - \left[\frac{0.4M_s^2 + 2}{2.8M_s^2 - 0.4} \right]^{\frac{1}{2}} .$$

If $M_s = 3$, then $M = 2.52$ and $\cot \delta = 11.5 \gg 2.3$. For smaller Mach numbers the margin of safety is even greater. For $M_s = 3$, the peak overpressure P is approximately 150 psi. Therefore, we were well within the requirements when we mounted the gauge on a unit for which $\delta = 5^\circ$.

c. Data Recording System

The instrumentation for recording the blast data was assembled and tested to establish that the requirements for precision, accuracy, and reliability were being satisfied. Figure 21 is a schematic diagram of the general system. Additional details are shown in Fig. 22.

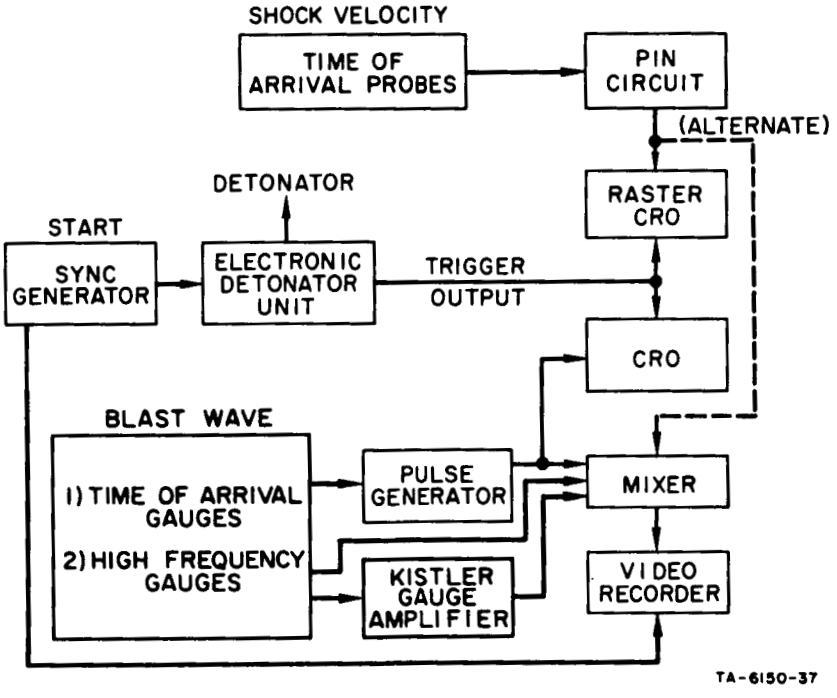

FIG. 21 SHOCK ATTENUATION AND BLAST WAVE MEASUREMENTS SYSTEM SCHEMATIC

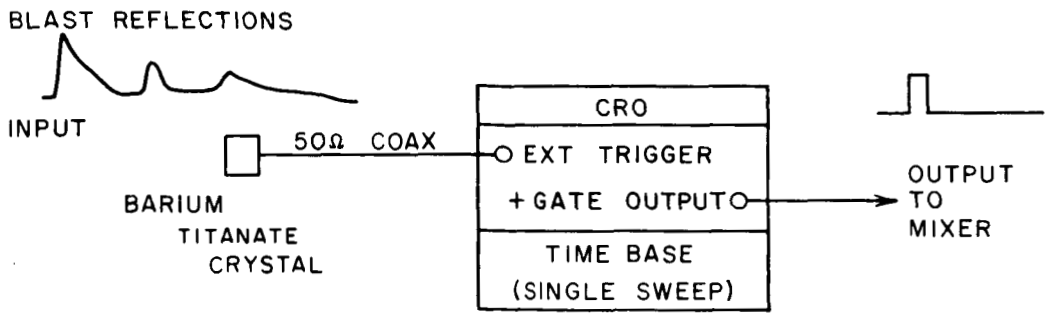

(a) ARRIVAL TIME MEASUREMENT

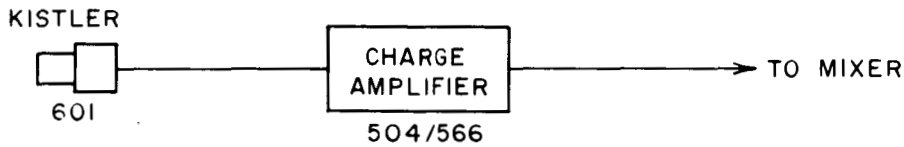

(b) BLAST PRESSURE MEASUREMENT

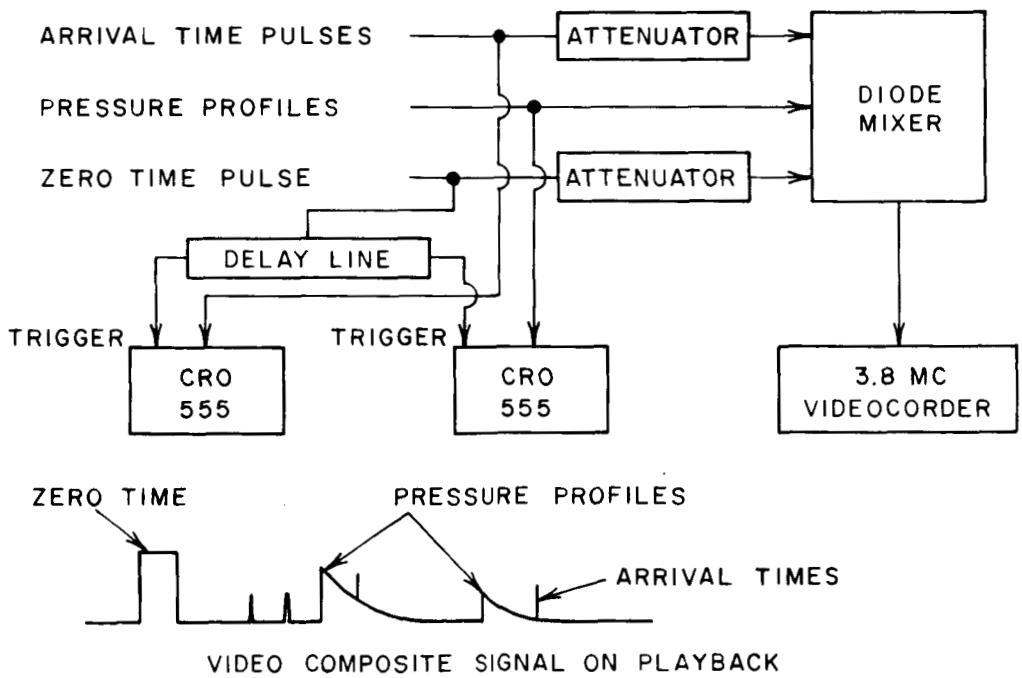

(c) PARAMETER RECORDER SYSTEM

TB-6150-5

FIG. 22 DETAILS OF DATA RECORDING SYSTEMS

The parameter recording system shown in Fig. 22(c) was used to adjust the gauge output amplitudes to a suitable level for the tape recorder. The output of the same system was also recorded on a set of precisely delayed oscilloscopes. The net effect was that the pressure and time-of-arrival data were recorded both on a wide band (30 to 3.8 Mc) videotape recorder for later playback (on an oscilloscope) and directly onto an oscilloscope. The redundancy gave improved reliability and accuracy.

3. Equivalence Factors from Time-of-Arrival Measurements

The experimental arrangement for determining the equivalence factor was basically very simple. The explosive charges used were combinations of two or three tetryl pellets (2 inches in diameter, 1 inch thick, 76.5 to 80 g*), with or without a 2-inch-diameter, 4-inch-long cylinder of propellant in contact. The tetryl was initiated by a cap and booster containing about 1 g explosive. Time-of-arrival gauges were placed in a line through the approximate center of the tetryl charge and perpendicular to the direction of detonation. Four gauges, 14 inches apart, were permanently mounted on a steel strip to assure both accuracy and reproducibility. The leading gauge was placed about 40 inches from the center of the charge, the exact distance (± 1/8 inch) being determined before each shot. Unfortunately, it was not realized until after the experiments were completed that the weights of the tetryl pellets varied perhaps by as much as 10%; hence the exact charge weight for each shot is not known.

*Mass range was based on 5 randomly chosen pellets.

The time of arrival, t, of the shock front at each gauge was recorded as previously described and the results were fitted to a curve of the form

$$\ell n\ t = A + B\ \ell n\ r + C(\ell n\ r)^2$$

for each shot; the three constants A, B, C were determined from the four measured pairs of values (log t, log r) for a best least-square fit. The shock velocity as a function of r is then given by

$$V \equiv \frac{dr}{dt} = \frac{d\ \ell n\ r}{d\ \ell n\ t} \cdot \frac{r}{t} = \frac{r}{(B + 2C\ \ell n\ r)\ \exp[A + B\ \ell n\ r + C(\ell n\ r)^2]}$$

from which the Mach number (V/c_o) and the peak overpressure

$$P + \frac{7[(V/c_o)^2 - 1]}{6} P_o$$

can be readily determined. (c_o and P_o are the ambient sound speed and pressure of the atmosphere.) Tables of P versus r were computed and printed out for small enough intervals of r to allow the determination of the value of r corresponding to a given P by inspection to the nearest tenth of an inch.

Shots were fired on two successive days, the eight shots of the first day being designated as Series I, the remaining four shots as Series II. Typical time-of-arrival data and fitted curves are shown in Fig. 23 for a shot with two tetryl pellets (No. 1) and a shot with two

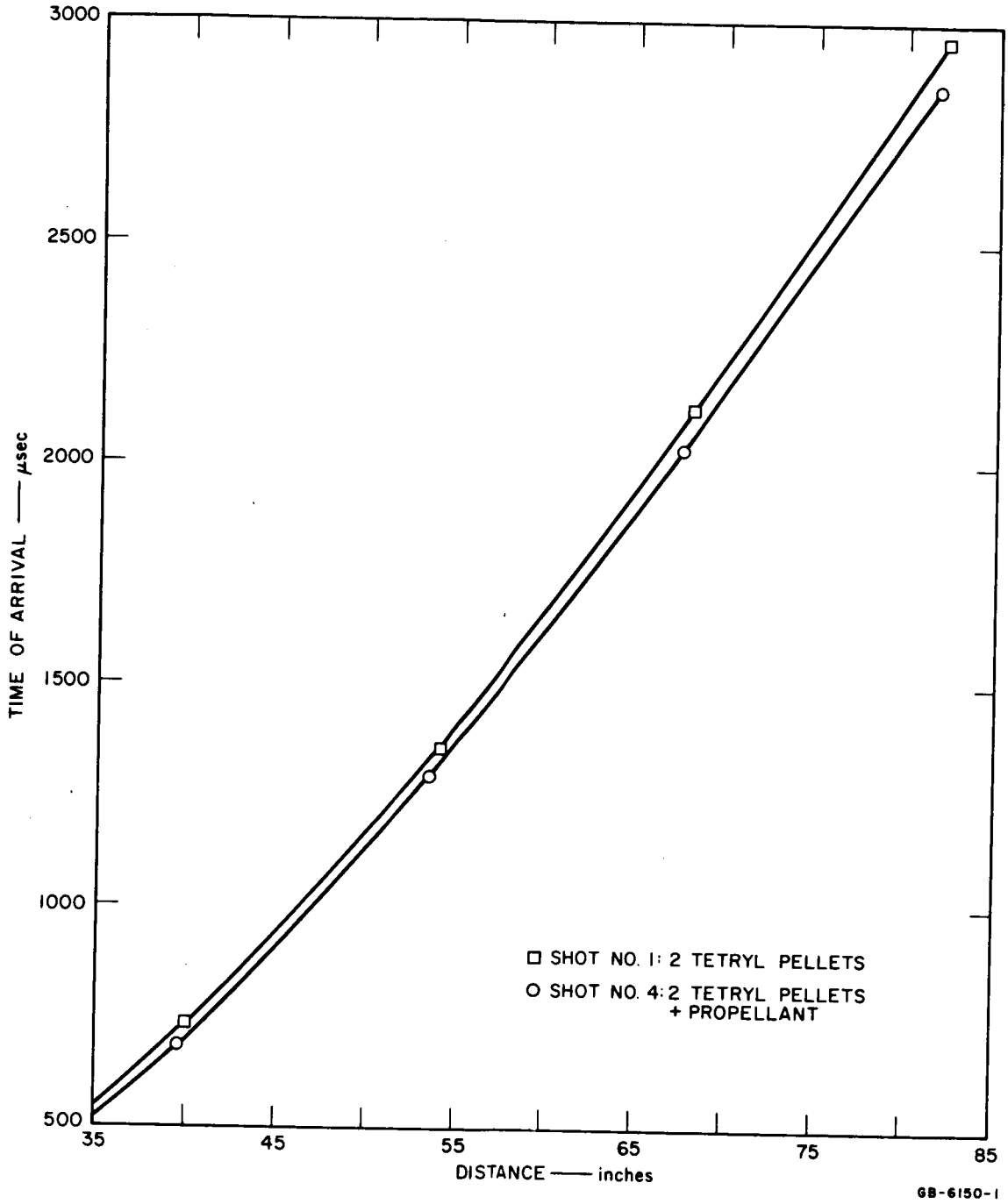

FIG. 23 AIR BLAST: TYPICAL TIME-OF-ARRIVAL MEASUREMENTS

tetryl pellets plus propellant (No. 4).* The distances corresponding to overpressures of 10, 20, 30, and 40 psi (derived from the fitted curves as explained above) are shown for all twelve shots in Table VIII. The agreement of results between two different shots of the same type fired on the same day is quite good, except perhaps at 10 psi where the distance as a function of overpressure varies rapidly; this pressure level was therefore not used in the calculation of equivalence factors. Shot No. 8 was similar to the propellant shots except that the propellant was replaced by a Lucite cylinder of the same dimensions; the results (except at 10 psi) fall well within the range of Shot Nos. 1, 2, and 5, indicating that whatever contribution the propellant makes to the blast is not purely mechanical.

In spite of the internal consistency within each series, there is an obvious disagreement between the results of Series I and Series II; nominally identical shots in Series II appear to produce weaker blasts (smaller r for a given overpressure), giving an indication of some systematic error. Fortunately, the method of calculating equivalence factors is such that if a similar error is made in all experiments used in a particular determination of f, this error will affect the equivalence factor only to second order, and this is the reason for dividing the shots into the two series.

---

*With only four experimental points per shot and three available constants in the fitting function, it is not surprising that the maximum deviation of the fit encountered in any shot was only 14 μsec.

TABLE VIII

DISTANCE AS A FUNCTION OF OVERPRESSURE

Type of Shot	Shot No.	Distance (inches) for given overpressure			
		10 psi	20 psi	30 psi	40 psi
Series I					
2 Tetryl Pellets	1	69.4	53.9	46.0	41.0
	2	70.5	53.5	45.7	40.7
	5*	68.4	52.3	44.4	39.8
Mean			53.7	45.8	40.8
3 Tetryl Pellets	3	76.7	61.8	53.5	48.0
	7	76.1	61.4	53.2	47.7
Mean			61.6	53.3	47.8
2 Tetryl Pellets	4	72.8	55.2	47.1	42.0
plus propellant	6	68.4	55.0	47.7	43.0
Mean			55.1	47.4	42.5
2 Tetryl Pellets plus Lucite	8	71.1	52.8	45.0	40.2
Series II					
2 Tetryl Pellets	9	67.0	51.0	43.4	38.7
	11	65.5	50.9	43.5	38.8
Mean			50.9	43.4	38.7
2 Tetryl Pellets	10	70.0	53.9	46.0	41.2
plus propellant		70.5	53.0	45.4	40.8
Mean			53.4	45.7	41.0

*Values for this shot not used in computing the means

The computed values of the equivalence factor f relative to 2 tetryl pellets are shown in Table IX. For Series I, Shot Nos. 1 and 2 were used as standard because of the close agreement of their distance-pressure functions. If Shot Nos. 5 and 8 had been used as standard, the resulting f-values for this series would have been increased by about 7 percent. This would bring the f-values for tetryl plus propellant in line with those obtained from Series II; however, it would also increase the deviation of the f-value for 3 tetryl pellets from the predicted value, 1.5. In view of the uncertainty in the charge weights, the agreement of the stated f-values for tetryl plus propellant is quite good, and it is fair to conclude that the energy released by the propellant is about 10 to 20 percent of the energy released by two tetryl pellets.

TABLE IX

EXPERIMENTAL DETERMINATION OF EQUIVALENCE FACTOR f FOR PBAN-170 WITH TETRYL

Type of Shot	Equivalence Factor f Relative to Blast Produced by Two Tetryl Pellets			
	20 psi	30 psi	40 psi	Mean
Series I				
3 tetryl pellets[1]	1.51	1.58	1.61	1.57
2 tetryl pellets[1] plus propellant	1.08	1.10	1.13	1.10
Series II				
2 tetryl pellets[2] plus propellant	1.15	1.17	1.19	1.17

[1]Assuming Shot Nos. 1 and 2 as standard.

[2]Assuming Shot Nos. 9 and 11 as standard.

4. Kistler Gauge Measurements

Unlike the time-of-arrival gauges, pressure gauges must be mounted with due regard to aerodynamic problems if they are to indicate the free-field overpressure. Although a single pressure gauge can be easily mounted on a suitable air foil, it is difficult to place several gauges in such a way that their relative distance from the center of explosion remains unchanged between shots without at the same time producing some aerodynamic interference among the gauges. Accordingly, the direct pressure measurements played a rather lesser role in the blast measurements than we had originally anticipated, and served primarily as a rough check on the time-of-arrival measurements. In Table X are shown the pressure readings obtained during eleven of the twelve shots from a Kistler gauge mounted well away from the time-of-arrival gauges. The agreement with the values obtained from the time-of-arrival measurements is seen to be quite good.

TABLE X

COMPARISON OF OVERPRESSURES OBTAINED
FROM KISTLER AND TIME-OF-ARRIVAL MEASUREMENTS

Shot No.	Distance in.	Overpressure Kistler (psi)	Overpressure Time of Arrival (psi)
Series I			
2	44.0	31.1	32.8
3	44.5	44.0	48.8
4	44.1	36.9	35.3
5	44.2	28.9	30.3
6	44.2	34.4	37.1
7	44.2	47.3	49.0
8	44.2	32.2	31.2
Series II			
9	44.7	31.3	28.5
10	44.5	34.4	32.6
11	44.9	28.4	27.6
12	44.5	34.3	31.7

F. Propellant Destroyed by Explosion

1. Sample Recovery

To relate the blast measurements to the amount of propellant destroyed or consumed, we recovered those parts of several shocked propellant cylinders that remained intact after the blast pressure experiments. These are shown in Fig. 24; the numbers before each specimen represent the initial propellant charge length in inches. In each case approximately $3\frac{1}{2}$ inches of the original length was not recovered. For reasons described later, similar tests were conducted with a dummy propellant and with the PBAN binder. The results from 4 inch cylinders are shown in Fig. 25. From these experiments we concluded that the amount consumed was independent of charge length and, approximately, a function of the binder properties only. It is important to note that all of these tests were performed with charges so long that the equivalence factor was independent of length.

Because these measurements were crude, we also used flash radiography to study the fragmentation process.

2. Flash Radiography

In formulating the research plan our hypothesis was that the processes occurring immediately behind the shock wave in a propellant could be described by assuming essentially hydrostatic behavior of the propellant. The consequences of this approach are best illustrated with the following sketch:

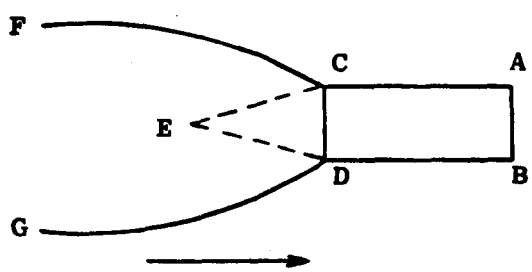

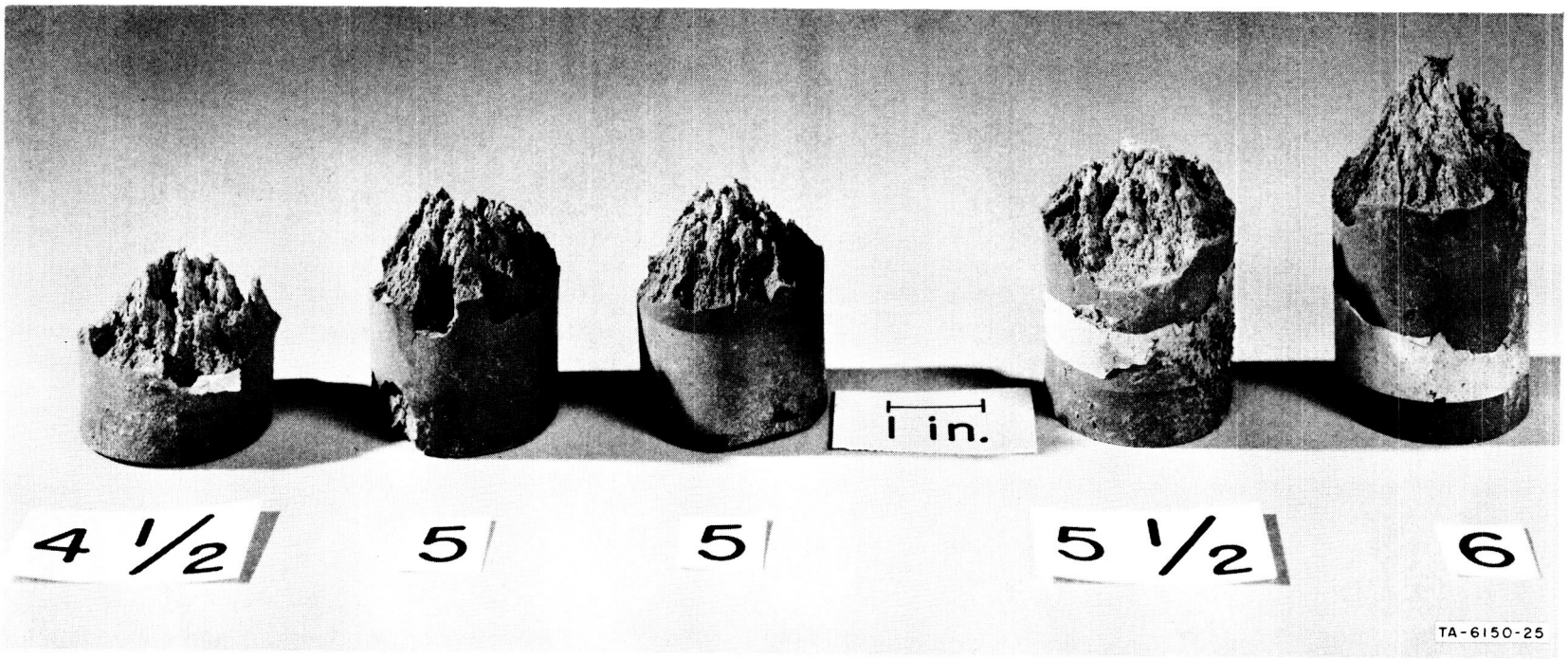

FIG. 24 RECOVERED PROPELLANT SAMPLES

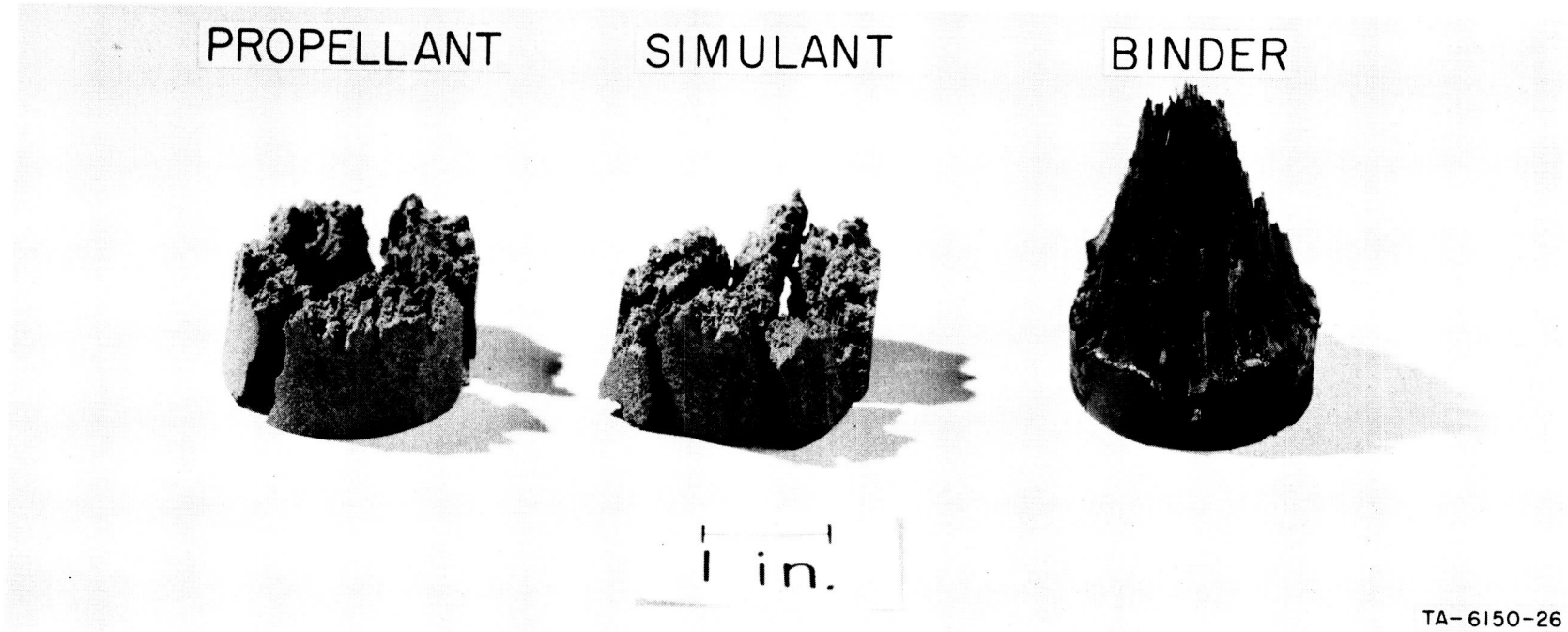

FIG. 25 RECOVERED SPECIMENS

ABDC is the unshocked propellant into which a slightly convex shock wave CD is traveling in the direction indicated by the arrow. Behind CD the shocked material expands laterally with the material fronts along CF and DG. Within a region CED the forward material velocity is uniform and has a value predicted from hydrodynamics. Behind this zone, i.e., behind FCEDG, this velocity begins to decay. It is in this regime that we expected fragmentation to occur.

Because of the dependence of subsequent behavior upon the decaying velocity and pressure just behind CD, there is some critical position of CD past which fragmentation would not be expected. To determine this position, propellant cylinders were X-rayed while they were being shocked. The geometry used is essentially that shown in Fig. 6; the only changes were to dispense with the ion probe and $BaTiO_3$ crystal and to use a 4 inch long cylinder of PBAN-170. The pictures obtained are shown in Fig. 26. The noted times are those elapsed from the instant of initiation; the shock wave is moving from the top to the bottom in each frame. At 64 μsec, a shadow is cast by a strip of solder inserted to check the focus, and at 37, 64, 75, and 125 μsec, the exposure of the unshocked propellant is super-imposed upon the shocked sample. Some details are lost in the reproduction process, but each original negative shows the phenomenon readily observed in the pictures taken after 37, 47, 64, and 75 μsec. Within the linear response range of the film, X-ray density is proportional to material density (<u>not</u> pressure), and we see an abrupt increase in density well behind the leading shock wave. This is noted by the arrows in the figures.

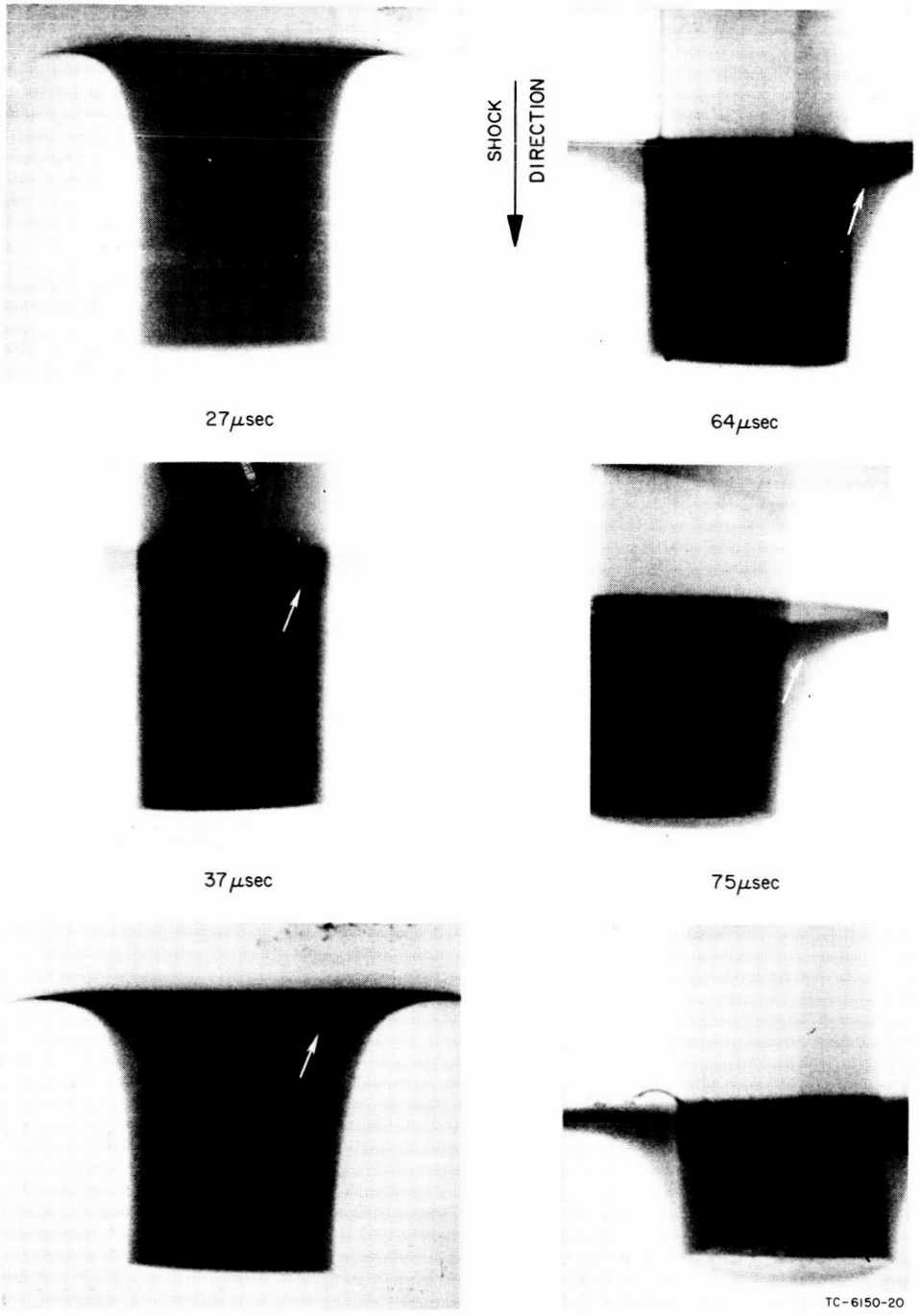

FIG. 26 FLASH RADIOGRAPHS OF SHOCKED PROPELLANT

This step-function in the density is not predicted by our simple model and, to our knowledge, has never before been observed in any material. It is customary to assume that all materials behave hydrostatically at these high pressures. We have no explanation for this abnormal behavior, but to determine whether the oxidizer plays an essential role we conducted similar experiments with (a) PBAN binder only, and (b) PBAN with glass beads to simulate PBAN-170. The same qualitative features appear in the X-rays: for both types of materials a step in the recorded density appeared at some distance behind the shock wave. We conclude, therefore, that this most unexpected behavior is a consequence of binder property and not of some binder-solid or binder-oxidizer interaction. (An attempt to relate the position of these waves to the time from initiation was made. Because of parallax and other errors the derived data could not be interpreted with sufficient precision; therefore, they are not included here nor are they plotted in Fig. 8.)

G. Stress Field Calculations in a Finite Diameter Cylinder*

Early thoughts about theoretical approaches to the problem of propellant detonation were based on two premises: (1) the propellant will behave like a brittle solid under dynamic loading, as many other plastics are known to do; (2) at low stress levels, detonation or explosion will occur slightly above the stress levels at which fractures

*This section was prepared by Professor George E. Duvall, Washington State University, a consultant on this project.

are initiated. From the experiments reported above, it appears that both premises are probably false with respect to the materials being investigated. Whether they are false for all propellant materials under all conditions is not known.

Using these premises, we undertook a numerical investigation of the dynamic stresses to be expected in the propellant cylinder. The intent of this investigation was to maximize the information obtained and to minimize the cost by taking full advantage of both premises. These imply that elastic calculations of the transient stresses induced in the cylinder are adequate to define the regions of maximum tensile stress which develop as the wave passes through the cylinder. Such regions could then be identified as the regions in which fractures first occur, and subsequent experimental investigations would concentrate on these critical regions. The implementation of this program was particularly simple. A computer program for calculating displacement in a finite, cylindrical, elastic bar has recently been developed[17] and has been adapted to this particular problem at nominal cost (see Appendix). In brief, the program calculates dynamic displacements in a cylindrical bar with a stress-free, radial surface, for uniform pressure with arbitrary time variation applied at one end and either fixed or free boundary at the other end.

Before extended machine runs were made, the experimental results indicated that the premises on which calculations were based were false (see, e.g., the radiographs in Fig. 26). Therefore, further efforts in this direction were abandoned.

The initial goal of this theoretical effort--to calculate detailed material states in the dynamic experiment--is still considered a valid one. It is now apparent that to achieve this goal requires a more general two-dimensional program for viscoelastic, reacting solids with finite stresses. The question remains whether or not some existing program can be adapted to this purpose at a cost commensurate with the total effort on the program.

V SUMMARY AND CONCLUSIONS

The following have been accomplished:

a. Precise shock attenuation measurements have been made in PBAN-170 with a particular geometry.

b. The Hugoniot for PBAN-170 has been obtained over the range 0 to 100 kbar.

c. Model explosions have been initiated and careful blast measurements made and analyzed.

d. The propellant remaining after the model explosions has been recovered and estimates made of the fraction of the original charge destroyed.

e. Flash radiographs were taken during the explosion.

f. Certain incidental measurements were made; these include the sonic velocity, mechanical properties, and burning rate of PBAN-170.

The attenuation data conform precisely to the predicted behavior: velocity attenuates exponentially. The Hugoniot shows neither anomalies nor plastic-elastic transition. However, low pressure Hugoniot data are often imprecise, and the absence of special features in our data should not be considered conclusive. The blast measurements indicate rather reproducibly that only a very small fraction of the propellant destroyed contributes to the blast wave. Lastly, unusual features of the flash radiographs remain to be explained.

From the Hugoniot and the attenuation data we compute that the pressure $3\frac{1}{2}$ inches down the propellant stick (where fragmentation ceases) is approximately 10 kbar. However, the contribution of the propellant to the blast by no means accounts for all of the propellant destroyed; in fact only about 5% of the unrecovered propellant appears to have so contributed. Furthermore, because of the concordance of our results with those obtained by Jaffe et al.[7] for Lucite, it is apparent that over the entire range within which precise measurements were made the shock attenuates without evidence of chemical support. Immediately, therefore, we can draw the following conclusions:

(a) Only a small fraction of the amount of material fragmented by the donor shock contributes to the blast.

(b) No large quantity of the propellant detonates.

Similarly, we can feel fairly certain about the following:

(a) For the materials and geometry studied the fraction of material fragmented may be determined by the mechanical properties of the binder alone, and not of the other components or the interfacial strengths.

(b) The small blast contribution from the propellant results from either an overdriven detonation in the portion of the propellant near the donor interface (likely) or rapid burning of a small fraction of each resultant fragment (also likely) or some combination of the two.

We still cannot speculate on the relation of the fraction fragmented to the mechanical properties except insofar as we have evaluated the shock pressure below which fragmentation apparently does not occur. The

experimentally determined Hugoniot shows neither anomalies nor plastic-elastic transition, but the flash radiographs do suggest anomalous behavior.

Thus our research has answered some of the questions posed by the model we set out to examine, and has raised significant new questions:

(a) What is the explanation for the anomalous radiographs and does it account for or bear on propellant fracture?

(b) Is the propellant blast contribution attributable to an overdriven detonation or to rapid surface burning of the propellant fragments?

REFERENCES

1. A. B. Amster, E. C. Noonan, and G. J. Bryan, "Solid Propellant Detonability," ARS J. 30, 960 (1960).

2. D. Price, "Dependence of Damage Effects upon Detonation Parameters of Organic High Explosives," Chem. Rev. 59, 801-825 (1959).

3. J. Taylor, "Detonation in Condensed Explosives," Oxford, Clarendon Press (1952).

4. J. A. Charest, B. H. Bichot, and J. S. Rinehart, "A Determination of the Dynamic Tensile Strength and Shock Attenuation of Simulated Solid Rocket Propellant," Technical Report MRL-ONR-1, Colorado School of Mines, 1 August 1963.

5. Explosion Effects Data Sheets, NAVORD Report 2986 (with changes), U. S. Naval Ordnance Laboratory, White Oak, Md., 14 June 1955.

6. J. N. Bradley, Shock Waves in Chemistry and Physics, John Wiley, New York, 1962, Chap. IV

7. I. Jaffe, R. Beauregard, and A. Amster, "Determination of the Shock Pressure Required to Initiate Detonation of an Acceptor in the Shock Sensitivity Test," ARS J. 32, 22 (1962).

8. R. C. Gottleman and M. W. Evans, "Longitudinal Sound Velocity in Columns of Granular Ammonium Perchlorate of Low Loading Density," Nature 198, 679 (1963)

9. M. H. Rice, R. G. McQueen, and J. M. Walsh, "Compression of Solids by Strong Shock Waves," in Solid State Physics, Vol. 6, Academic Press, New York, 1958.

10. G. E. Duvall, Shock Waves in Solids, Modern Science and Technology, R. Colburn, ed. D. Van Nostrand & Co., Princeton, New Jersey, 1965.

11. G. R. Fowles, "Shock Wave Compression of Hardened and Annealed 2024 Aluminum," J. Appl. Phys. 32, 1475 (1961)

12. M. W. Evans and D. N. Schmidt, "Wave Compression of Plexiglas in the 2.5 to 20 Kilobar Region," Nature 206, 1348 (1965)

13. W. C. Holton, "The Detonation Pressure in Explosives as Measured by Transmitted Shocks in Water," NAVORD Report 3968, December 1954 (CONFIDENTIAL)

14. M. A. Cook, R. T. Keyes, and W. O. Ursenbach, "Measurements of Detonation Pressure," J. Appl. Phys. 33, 3413 (1962)

15. N. L. Coleburn, "Sensitivity of Composite and Double-Base Propellants to Shock Waves," AIAA J. 4, 521 (1966)

16. R. H. Cole, Underwater Explosions, Dover, New York 1965, p. 178

17. L. D. Bertholf, "Numerical Solution for Two-Dimensional Elastic Wave Propagation in Finite Bars," to be published in J. Appl. Mechanics

18. S. R. Brinkley, Jr., "Blast Effects from Propellant Explosions," Summary of 1964 Conference on Large Solid Motor Explosion Hazards, SSD-TDR-64-256, prepared under Contract AF04(695)-269, 10 November 1964, pp. 15-19.

19. S. R. Brinkley, Jr. and J. Kirkwood, "Theory of the Propagation of Shock Waves," Phys. Rev. 71, 606 (1947)

APPENDIX

COMPUTER PROGRAM FOR ELASTIC WAVE PROPAGATION FINITE CYLINDRICAL BAR

The material in this appendix has been taken from a Ph.D. Thesis by L. D. Bertholf, "Longitudinal Elastic Wave Propagation in Finite Cylindrical Bars," WSU SDL 66-03, Shock Dynamics Laboratory, Washington State University, Pullman, Washington, July, 1966.

FLOW CHART

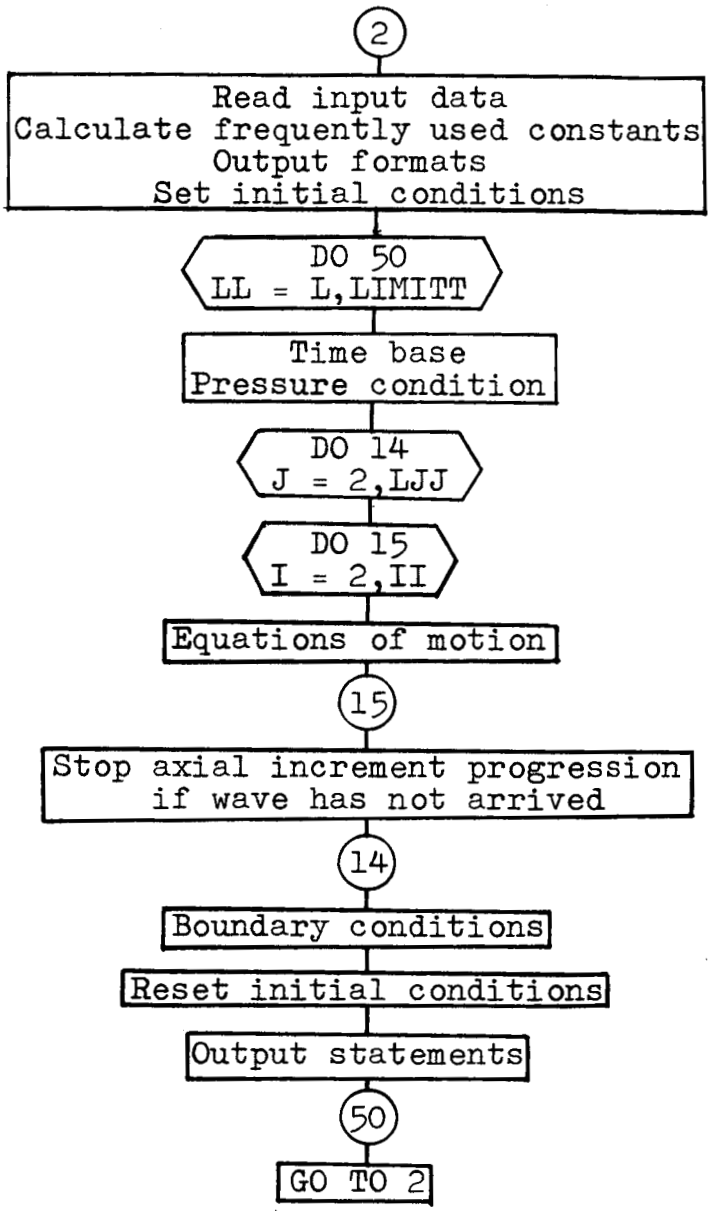

Card Numbers	
2DBAR003	
2DBAR004	2DBAR036
2DBAR037	
2DBAR038	2DBAR040
2DBAR041	
2DBAR042	
2DBAR043	2DBAR066
2DBAR067	
2DBAR068	2DBAR071
2DBAR072	
2DBAR074	2DBAR177
2DBAR178	2DBAR184
2DBAR185	2DBAR198
2DBAR199	
2DBAR201	

```
HERNDON                    SRI   P572                              DATE 01/19/67
$IBFTC TOCBAR                                                      2DBARC00

      DIMENSION  U(12,200,3) , W(12,200,3) ,          A(30,30), B(30),2DBARC01
     6X(30), AA(30,30), BB(30) , XX(30)                            2DBARC02
  2   CONTINUE                                                     2DBARC03
      TAUU = 6.0                                                   2DBARC04
      TIME = 0.0                                                   2DBARC04
      KKKKK= 0                                                     2DBARC04
      READ (5,1) MM,LIMITI,LIMITT,LIMITZ,JZCAL,JZWRT,PO,IBCD,DT,DR,DZ,  2DBARC05
     6XNU,E,RHO                                                    2DBARC06
  1   FORMAT (6I3,F9.4,I1, 6F7.6)                                  2DBARC07
      XMU = E/(2. *(1. + XNU))                                     2DBARC08
      XLAMB = E*XNU/(( 1. -2. *XNU)*(1. + XNU))                    2DBARC09
      G = XLAMB/(XLAMB+ 2.* XMU)                                   2DBARC10
      LJ = LIMITZ                                                  2DBARC11
      LJJ = LIMITZ -1                                              2DBARC12
      DTT = DT**2                                                  2DBARC13
      II= LIMITI -1                                                2DBARC14
      III = LIMITI -2                                              2DBARC15
      CC = SQRT ((XLAMB + 2.* XMU)/RHO)                            2DBARC16
      WRITE (6,3)                                                  2DBARC17
  3   FORMAT (1H1,2X, 44HDISPLACEMENTS, U(R) AND U(Z) IN CENTIMETERS.)  2DBARC18
      WRITE (6,5)                                                  2DBARC19
   5  FORMAT (/3X,21HTIME IN MICROSECONDS.  )                      2DBARC20
      WRITE (6,6)                                                  2DBARC21
   6  FORMAT(/3X,23HR AND Z IN CENTIMETERS.  )                     2DBARC22
      WRITE (6,7)  XNU                                             2DBARC23
   7  FORMAT(/3X,18HPOISSON-S RATIO IS,F6.3,1H. )                  2DBARC24
      WRITE (6,9)  E                                               2DBARC25
  9   FORMAT(/3X,17HYOUNGS MODULUS IS,F6.3,8H(MBARS).)             2DBARC26
      WRITE (6,11)  RHO                                            2DBARC27
  11  FORMAT(/3X,10HDENSITY IS, F6.3, 8H(GM/CC).  )                2DBARC28
      WRITE (6,12)                                                 2DBARC29
  12  FORMAT(//////// ,3X,4HTIME,5X,1HR,6X,1HZ, 9X,4HPL(R), 12X,   2DBARC30
     14HU(Z),11X,5HSIGZZ,11X,5HSIGRR,10X,6HSIGPHP,11X,5HSIGRZ//)   2DBARC31
      DO 4 I= 1,LIMITI                                             2DBARC32
      DO 4 J= 1,LIMITZ                                             2DBARC33
      DO 4 K= 1,3                                                  2DBARC34
      W(I,J,K) = 0.                                                2DBARC35
   4  U(I,J,K) = 0.                                                2DBARC36
      DO 50 LL= 1,LIMITT                                           2DBARC37
      N=LL-1                                                       2DBARC38
      FN= N                                                        2DBARC39
      P = PO*EXP(-TIME/TAUU)                                       2DBARC040
      WRITE(6,8) TIME,P                                            2DBARC40
    8 FORMAT(////20X,7HTIME = ,F9.2,40X,4HP = ,E15.5////)          2DBARC40
      DO 14 J= 2,LJJ                                               2DBARC41
      DO 15 I= 2,II                                                2DBARC042
      R= DR*FLOAT(I-1)                                             2DBARC43
      UU222 = U(I,J,2)                                             2DBARC44
      WW222 = W(I,J,2)                                             2DBARC45
C     THIS IS THE BEGINNING OF THE DIFFERENTIAL EQUATIONS          2DBARC46
C     THIS IS THE BEGINNING OF THE DIFFERENTIAL EQUATIONS          2DBARC47
      U(I,J,3) = 2.* UU222    -U(I,J,1) + DTT*(                    2DBARC48
     6 (1.   /(4.* DZ*DR ))*((XLAMB + XMU)/RHO) *                  2DBARC49
     6 (W(I+1, J+1,2) - W(I-1, J+1,2) -W(I+1, J-1, 2) + W(I-1,J-1,2))  2DBARC050
     6  +(XMU/RHO)*(1.   /DZ**2)*(U(I,J+1 ,2) + U(I,J-1,2) - 2.*UU222  2DBARC51
```

```
     6  ) - ((XLAMB+2.*XMU)/RHC)* (1.    /R**2)*UU222                          2DBARC52
     6  *((XLAMB+ 2.*XMU)/RHC)*(1.    /DR**2)*                                 2DBARC53
     6 ( U(I+1, J,2) + U(I-1, J,2) -2.* UU222 )                               2DBARC54
     6 +((XLAMB+ 2.*XMU)/RHO)*(1.    /(2.*R*DR))*                             2DBARC55
     6 ( U(I+1,J,2) - U(I-1,J,2)))                                            2DBARC56
      W(I,J,3) = 2.* WW222     - W(I,J,1) + CTT*(                            2DBARC57
     6 (1.    /(4.* DZ*DR ))*((XLAMB + XMU)/RHC) *                            2DBARC58
     6 (U(I+1, J+1,2) - U(I-1, J+1,2) -U(I+1, J-1, 2) + U(I-1,J-1,2))        2DBARC59
     6 +((XLAMB+ XMU)/RHO)*(1.    /(2.*R*DZ))*                                2DBARC60
     6  (U(I,J+1,2) -U(I,J-1,2))          +                                  2DBARC61
     6 (XMU/RHO)*(1.    /DR**2)*                                              2DBARC62
     6 (W(I+1, J, 2) + W( I-1, J, 2) - 2.* WW222    )                         2DBARC63
     6 +(XMU/RHO)*(1.    /(2.*R*DR ))* (W(I+1,J,2) - W(I-1,J,2))              2DBARC64
     6 +((XLAMB +2.*XMU)/RHO) *(1.    /DZ**2)*                                2DBARC65
     6  ( W(I,J+1,2)  +W(I,J-1,2) -2.*WW222    ))                           2DBARC66
  15 CONTINUE                                                                 2DBARC67
C      THIS IS THE      END    OF THE DIFFERENTIAL EQUATIONS                   2DBARC68
C      THIS IS THE      END    OF THE DIFFERENTIAL EQUATIONS                   2DBARC69
       JJJ =1.25* CO*FM*DT/DZ                                                 2DBARC70
       IF ( J .GT. JJJ + JZCAL) GO TO 18                                      2DBARC71
  14 CONTINUE                                                                 2DBARC72
  18 CONTINUE                                                                 2DBARC73
       JJ=J +1                                                                2DBARC74
       INC = 1                                                                2DBARC75
C      THIS IS THE BEGINNING OF THE BOUNDARY CONDITIONS                       2DBARC76
C      THIS IS THE BEGINNING OF THE BOUNDARY CONDITIONS                       2DBARC77
C      BOUNDARY CONDITIONS FOR R=0                                            2DBARC78
       DO 89 J= 1,LIMITZ                                                      2DBARC79
       W(1,J,3) = W(2,J,3)                                                    2DBARC80
  89   U(1,J,3) = 0.                                                          2DBARC81
C      BOUNDARY CONDITIONS FOR R=0                                            2DBARC82
       IF(IBCD .EQ. 1) GO TO 799                                              2DBARC83
C      BOUNDARY CONDITIONS FOR FIXED END AT Z = L                             2DBARC84
       DO 35 I= 1,LIMITI                                                      2DBARC85
       W(I,LIMITZ, 3) = 0.                                                    2DBARC86
  35   U(I,LIMITZ,3) = U(I,LJJ,3)                                             2DBARC87
C      BOUNDARY CONDITIONS FOR FIXED END AT Z = L                             2DBARC88
  799 CONTINUE                                                                2DBARC89
       IF (IBCC .NE. 1) GO TO 789                                             2DBARC90
C      BOUNDARY CONDITIONS FOR  FREE END AT Z = L                             2DBAR091
       LLL = LL +1                                                            2DBAR092
       IF (LLL .LT. LIMITZ) GO TO 3000                                        2DBAR093
       KKKKK = KKKKK + 1                                                      2DBAR094
       BB(1) = W(1,LJJ,3)                                                     2DBAR095
       BB(22) = DR/DZ*G*W(11,LJJ,3)                                           2DBAR096
       DO 3333 I= 2,11                                                        2DBAR097
       BB(I) = W(I,LJJ,3)                                                     2DBAR098
       BB(I+10) = U(I,LJJ,3)                                                  2DBAR099
 3333 CONTINUE                                                                2DBAR100
       INN = 2                                                                2DBAR101
       IF (KKKKK . GT. 2) GO TO 4032                                          2DBAR102
       INN = 1                                                                2DBAR103
       DO 8888 I= 1,30                                                        2DBAR104
       DO 8888 J= 1,30                                                        2DBAR105
 8888 AA(I,J) = 0.                                                            2DBAR106
       AA(1,1) = 1.                                                           2DBAR107
       AA(1,12) = 2.*G*DZ/DR                                                  2DBAR108
       AA(22,22) = 1.                                                         2DBAR109
       AA(22,21) = G/10. -1.                                                  2DBAR110
```

```
      AA(22,10) = G*DR/DZ                                              2DBAR111
      DO 6655 I= 2,11                                                  2DBAR112
      AA(I,I-1) = 1.                                                   2DBAR113
      AA(I,I+11) = G*DZ/DR                                             2DBAR114
      AA(I,I+10) = G*DZ/DR*(1./FLOAT(I-1) -1.)                         2DBAR115
      AA(I+10,I+10) = 1.                                               2DBAR116
      AA(I+10,I) = DZ/DR                                               2DBAR117
      AA(I+10,I-1) =-DZ/DR                                             2DBAR118
 6655 CONTINUE                                                         2DBAR119
 4032 CONTINUE                                                         2DBAR120
      CALL SSOLVE (22, AA, BB, INN, 1.E-08, 10, XX, ITT)               2DBAR121
      DO 3005 I= 1,11                                                  2DBAR122
      W(I+1, LJ, 3) = XX(I)                                            2DBAR123
      U(I+1,LJ, 3) =XX(I+11)                                           2DBAR124
 3005 CONTINUE                                                         2DBAR125
      U(1, LJ, 3) = 0.                                                 2DBAR126
      W(1,LJ,3) =  W(2,LJ,3)                                           2DBAR127
 3000 CONTINUE                                                         2DBAR128
C     BOUNDARY CONDITIONS FOR  FREE END AT Z = L                       2DBAR129
  789 CONTINUE                                                         2DBAR130
C     BOUNDARY CONDITIONS FOR A PRESSURE APPLIED AT Z=0                2DBAR131
      B(1) = -P*G*DZ/XLAMB - W(1,2,3)                                  2DBAR132
      B(22) = -G*DR/DZ*W(11,2,3)                                       2DBAR133
      DO 2000 I= 2,11                                                  2DBAR134
      B(I) = -P*G*DZ/XLAMB - W(I,2,3)                                  2DBAR135
      B(I+10) = - U(I,2,3)                                             2DBAR136
 2000 CONTINUE                                                         2DBAR137
      IN = 2                                                           2DBAR138
      IF ( N.GT. 2 ) GO TO 2003                                        2DBAR139
      IN = 1                                                           2DBAR140
      DO 654 I= 1,30                                                   2DBAR141
      DO 654 J= 1,30                                                   2DBAR142
 654  A(I,J) = 0.0                                                     2DBAR143
      A(1,1) = -1.                                                     2DBAR144
      A(1,12) = G*2.*DZ/DR                                             2DBAR145
      A(22,22) = 1.                                                    2DBAR146

      A(22,21) = -1. + G/10.                                           2DBAR147
      A(22,10) = - G*DR/DZ                                             2DBAR148
      DO 6555 I=2,11                                                   2DBAR149
      A(I, I-1) = -1.                                                  2DBAR150
      A(I,I+11) = G*DZ/DR                                              2DBAR151
      A(I,I+10) = G*DZ/DR*(1./FLOAT (I-1)  - 1.)                       2DBAR152
      A(I+10, I) = DZ/DR                                               2DBAR153
      A(I+10, I-1) = - DZ/DR                                           2DBAR154
      A(I+10,I+10) = -1.                                               2DBAR155
 6555 CONTINUE                                                         2DBAR156
 2003 CONTINUE                                                         2DBAR157
      CALL SOLVE (22, A, B, IN, 1.E-08, 10,X,IT)                       2DBAR158
      DO 2005 I= 1,11                                                  2DBAR159
      W(I+1,1,3) = X(I)                                                2DBAR160
      U(I+1,1,3) = X(I+11)                                             2DBAR161
 2005 CONTINUE                                                         2DBAR162
      U(1,1,3) = 0.                                                    2DBAR163
      W(1,1,3) = W(2,1,3)                                              2DBAR164
C     BOUNDARY CONDITIONS FOR A PRESSURE APPLIED AT Z=0                2DBAR165
C     BOUNDARY CONDITIONS FOR RADIAL SURFACE                           2DBAR166
      DO 78 J= 2,JJ                                                    2DBAR167
```

```
      IF (J .EQ. LIMITZ) GO TO 567                                      2DBAR168
      U(LIMITI,J,3) = U(II ,J,3)-    G*U(II,J,3)/FLOAT(III)             2DBAR169
     6-   G*(DR/DZ)*(W(II,J+1,3) -W(II,J,3))                           2DBAR170
   78 W(LIMITI,J,3) = W(II ,J,3) -    DR/DZ*(U(II,J+1,3) -U(II,J,3))   2DBAR171
  567 CONTINUE                                                          2DBAR172
C     BOUNDARY CONDITIONS FOR RADIAL SURFACE                            2DBAR173
      IF (IBCC .NE. 1)  U(LIMITI,LJ,3) = U(II , LJ,3) - G   *U(II,LJ,3) 2DBAR174
     6/FLOAT(III) -   G*DR/DZ*(W(II,LJ,3) -W(II,LJJ,3))                 2DBAR175
C     THIS IS THE    END    OF THE BOUNDARY CONDITIONS                  2DBAR176
C     THIS IS THE    END    OF THE BOUNDARY CONDITIONS                  2DBAR177
      DO 3C I= 1,LIMITI                                                 2DBAR178
      DO 3C K= 1,JJ                                                     2DBAR179
      U(I,K,1) = U(I,K,2)                                               2DBAR180
      W(I,K,1) = W(I,K,2)                                               2DBAR181
      U(I,K,2) = U(I,K,3)                                               2DBAR182
   31 W(I,K,2) = W(I,K,3)                                               2DBAR183
   3C CONTINUE                                                          2DBAR184
      IF (N.GT. LIMITT - 4) INC = 1                                     2DBAR185
      IF (N .LT. 15 .AND. IBCC .EQ. 1) INC = 1                          2DBAR186
      MMM = MM*(N/MM)                                                   2DBAR187
      IF(N .NE. MMM )   GO TO 41                                        2DBAR188
      TIME =DT* FM                                                      2DBAR189
      DO 4C K= 1,JJ,JZWRT                                               2DBAR190
      DO 4C I= INC, LIMITI, INC                                         2DBAR191
      Z=DZ*FLOAT(K-1)                                                   2DBAR192
      R=DR* FLOAT(I-1)                                                  2DBAR193
      EPS = (W(I,K+1, 2) - W(I,K,2))/DZ                                 2DBAR194
      EZZ = EPS                                                         2DBAR194
      ERR = (U(I+1,K,2) - U(I,K,2))/DR                                  2DBAR194
      EPHPH = 0.0                                                       2DBAR194
      IF (I .NE. 1) EPHPH = U(I,K,2)/R                                  2DBAR194
      ERZ = 0.5*((W(I+1,K,2) - W(I,K,2))/DR + (U(I,K+1,2) - U(I,K,2))   2DBAR194
     1       /DZ)                                                       2DBAR194
      THETA = ERR + EZZ + EPHPH                                         2DBAR195
C     CALCULATE 2.0*XMU AND XLAMB*THETA AND STORE                       2DBAR195

      SIGRZ = XMU + XMU                                                 2DBAR195
      SIGPHP = XLAMB*THETA                                              2DBAR195
      SIGRR = SIGRZ*ERR + SIGPHP                                        2DBAR195
      SIGZZ = SIGRZ*EZZ + SIGPHP                                        2DBAR195
      SIGPHP = SIGRZ*EPHPH + SIGPHP                                     2DBAR195
      SIGRZ = SIGRZ*ERZ
      WRITE(6,45) TIME,R,Z,U(I,K,2),W(I,K,2),SIGZZ,SIGRR,               2DBAR195
     1            SIGPHP,SIGRZ                                          2DBAR195
   45 FORMAT(1X,3F7.3,6E16.7)                                           2DBAR196
   4C CONTINUE                                                          2DBAR197
   41 CONTINUE                                                          2DBAR198
   5C CONTINUE                                                          2DBAR199
   6C CONTINUE                                                          2DBAR2CC
      RETURN                                                            2DBAR2C2
      END                                                               2DBAR203
```

```
$IBFTC SOLLVE                                                    SLV40C00
C
CSOLVE   LINEAR EQUATION SOLVER WITH ITERATIVE IMPROVEMENT   VERSION IV SLV40010
      SUBROUTINE SOLVE(NN,A,B,IN,EPS,ITMAX,X,IT)                 SLV40020
C     SOLVES AX=B WHERE A IS NXN MATRIX AND B IS NX1 VECTOR      SLV40030
C     IN=                                                        SLV40040
C         1 FOR FIRST ENTRY                                      SLV40050
C         2 FOR SUBSEQUENT ENTRIES WITH NEW B                    SLV40060
C         3 TO RESTORE A AND B                                   SLV40070
C     EPS AND ITMAX ARE PARAMETERS IN THE ITERATION              SLV40080
C     IT=                                                        SLV40090
C         -1 IF A IS SINGULAR                                    SLV40100
C         0 IF NOT CONVERGENT                                    SLV40110
C         NUMBER OF ITERATIONS IF CONVERGENT                     SLV40120
C     CALLS MAP SUBROUTINES ILOG2,DOT,SDOT AND DAD               SLV40130
C                                                                SLV40140
C     TO MODIFY DIMENSIONS, CHANGE THE NEXT 3 (NOT 2 BUT 3) CARDS. SLV40150
      DIMENSION A(30,30),B(30),X(30),AA(30,30),DX(30),R(30),     SLV40160
     *          Z(30),RM(30),IRP(30)                             SLV40170
      MA=30                                                      SLV40180
C     MA MUST = DECLARED DIMENSION OF SYSTEM                     SLV40190
      EQUIVALENCE(R,DX)                                          SLV40200
      GO TO (1000,2000,3000),IN                                  SLV40210
 1000 N=NN                                                       SLV40220
      NM1=N-1                                                    SLV40230
      NP1=N+1                                                    SLV40240
C                                                                SLV40250
C     EQUILIBRATION                                              SLV40260
C                                                                SLV40270
      DO 510 I=1,N                                               SLV40280
          KTOP=ILOG2(A(I,1))                                     SLV40290
          DO 503 J=2,N                                           SLV40300
  503     KTOP=MAXO(KTOP,ILOG2(A(I,J)))                          SLV40310
          RM(I)=2.0**(-KTOP)                                     SLV40320
          DO 509 J=1,N                                           SLV40330
  509     A(I,J)=A(I,J)*RM(I)                                    SLV40340
  510 CONTINUE                                                   SLV40350
C                                                                SLV40360
C     SAVE EQUILIBRATED DATA                                     SLV40370
C                                                                SLV40380
      DO 548 I=1,N                                               SLV40390
      DO 548 J=1,N                                               SLV40400
  548 AA(I,J)=A(I,J)                                             SLV40410
C                                                                SLV40420
C     GAUSSIAN ELIMINATION WITH PARTIAL PIVOTING                 SLV40430
C                                                                SLV40440
      DO 99 M=1,NM1                                              SLV40450
          TOP=ABS (A(M,M))                                       SLV40460
          IMAX=M                                                 SLV40470
          DO 12 I=M,N                                            SLV40480
               IF(TOP-ABS (A(I,M)))10,12,12                      SLV40490
   10          TOP=ABS (A(I,M))                                  SLV40500
               IMAX=I                                            SLV40510
   12     CONTINUE                                               SLV40520
          IF(TOP)14,13,14                                        SLV40530
   13     IT=-1                                                  SLV40540
C         *SINGULAR*                                             SLV40550
```

```
      RETURN                                                          SLV40560
   14 IRP(M)=IMAX                                                     SLV40570
   23 IF(IMAX-M)29,29,24                                              SLV40580
   24 DO 25 J=1,N                                                     SLV40590
         TEMP=A(M,J)                                                 SLV40600
         A(M,J)=A(IMAX,J)                                            SLV40610
   25    A(IMAX,J)=TEMP                                              SLV40620
   29 MP1=M+1                                                         SLV40630
      DO 33 I=MP1,N                                                  SLV40640
         EM=A(I,M)/A(M,M)                                            SLV40650
         A(I,M)=EM                                                   SLV40660
         IF(EM)31,33,31                                              SLV40670
   31    DO 32 J=MP1,N                                               SLV40680
   32    A(I,J)=A(I,J)-A(M,J)*EM                                     SLV40690
   33 CONTINUE                                                        SLV40700
   99 CONTINUE                                                        SLV40710
      IRP(N)=N                                                        SLV40720
      IF (A(N,N))120,113,120                                          SLV40730
  113 IT=-1                                                           SLV40740
      RETURN                                                          SLV40750
  120 CONTINUE                                                        SLV40760
C     STORAGE FOR A NOW CONTAINS TRIANGULAR L AND U SO THAT (L+I)*U=A  SLV40770
C                                                                     SLV40780
C     DUPLICATE INTERCHANGES IN DATA                                  SLV40790
C                                                                     SLV40800
      DO 229 I=1,N                                                    SLV40810
         IP=IRP(I)                                                    SLV40820
         IF(I-IP)221,229,221                                          SLV40830
  221    DO 222 J=1,N                                                SLV40840
            TEMP=AA(I,J)                                             SLV40850
            AA(I,J)=AA(IP,J)                                         SLV40860
  222       AA(IP,J)=TEMP                                            SLV40870
  229 CONTINUE                                                        SLV40880
C                                                                     SLV40890
C     PROCESS RIGHT HAND SIDE                                         SLV40900
C                                                                     SLV40910
 2000 CONTINUE                                                        SLV40920
      DO 601 I=1,N                                                    SLV40930
  601    B(I)=B(I)*RM(I)                                              SLV40940
      DO 609 I=1,NM1                                                  SLV40950
         IP=IRP(I)                                                    SLV40960
         TEMP=B(I)                                                    SLV40970
         B(I)=B(IP)                                                   SLV40980
         B(IP)=TEMP                                                   SLV40990
  609 CONTINUE                                                        SLV41000
C                                                                     SLV41010
C     SOLVE FOR FIRST APPROXIMATION TO X                              SLV41020
C                                                                     SLV41030
  199 DO 200 I=1,N                                                    SLV41040
  200 Z(I)=-SDOT(I-1,A(I,1),MA,Z(1),1,-B(I))                          SLV41050
      DO 201 K=1,N                                                    SLV41060
      I=NP1-K                                                         SLV41070
  201 X(I)=-SDOT(N-I,A(I,I+1),MA,X(I+1),1,-Z(I))/A(I,I)               SLV41080
C                                                                     SLV41090
C     ITERATIVE IMPROVEMENT                                           SLV41100
C                                                                     SLV41110
```

```
      IF(ITMAX)370,370,300                                          SLV41120
  300 TOP=0.0                                                       SLV41130
      DO 303 I=1,N                                                  SLV41140
  303 TOP=AMAX1(TOP,ABS(X(I)))                                      SLV41150
      EPSX=EPS*TOP                                                  SLV41160
      DO 369 IT=1,ITMAX                                             SLV41170
C         FIND RESIDUALS                                            SLV41180
          DO 319 I=1,N                                              SLV41190
  319     R(I)=-DOT(N,AA(I,1),MA,X(1),1,-B(I))                      SLV41200
C         FIND INCREMENT                                            SLV41210
          DO 329 I=1,N                                              SLV41220
  329     Z(I)=-SDOT(I-1,A(I,1),MA,Z(1),1,-R(I))                    SLV41230
          DO 339 K=1,N                                              SLV41240
          I=NP1-K                                                   SLV41250
  339     DX(I)=-SDOT(N-I,A(I,I+1),MA,DX(I+1),1,-Z(I))/A(I,I)       SLV41260
C         INCREMENT AND TEST CONVERGENCE                            SLV41270
          TOP=0.0                                                   SLV41280
          DO 342 I=1,N                                              SLV41290
               TEMP=X(I)                                            SLV41300
               X(I)=DAD(X(I),DX(I))                                 SLV41310
               DELX=ABS (X(I)-TEMP)                                 SLV41320
               TOP=AMAX1(TOP,DELX)                                  SLV41330
  342     CONTINUE                                                  SLV41340
          IF(TOP-EPSX)381,381,369                                   SLV41350
  369 CONTINUE                                                      SLV41360
  370 IT=0                                                          SLV41370
  381 RETURN                                                        SLV41380
C                                                                   SLV41390
C     RESTORE A AND B                                               SLV41400
C                                                                   SLV41410
 3000 CONTINUE                                                      SLV41420
      DO 709 K=1,N                                                  SLV41430
          I=NP1-K                                                   SLV41440
          IP=IRP(I)                                                 SLV41450
          IF(I-IP)701,709,701                                       SLV41460
  701     TEMP=B(I)                                                 SLV41470
          B(I)=B(IP)                                                SLV41480
          B(IP)=TEMP                                                SLV41490
          DO 702 J=1,N                                              SLV41500
               TEMP=AA(I,J)                                         SLV41510
               AA(I,J)=AA(IP,J)                                     SLV41520
  702          AA(IP,J)=TEMP                                        SLV41530
  709 CONTINUE                                                      SLV41540
      DO 729 I=1,N                                                  SLV41550
          B(I)=B(I)/RM(I)                                           SLV41560
          DO 729 J=1,N                                              SLV41570
          A(I,J)=AA(I,J)/RM(I)                                      SLV41580
  729 CONTINUE                                                      SLV41590
      RETURN                                                        SLV41600
      END                                                           SLV41610
```

SAMPLE OUTPUT

DISPLACEMENTS, U(R) AND U(Z) IN CENTIMETERS.

TIME IN MICROSECONDS.

R AND Z IN CENTIMETERS.

POISSON-S RATIO IS 0.460.

YOUNGS MODULUS IS 0.024(MBARS).

DENSITY IS 1.690(GM/CC).

TIME	R	Z	U(R)	U(Z)	SIGZZ	SIGRR	SIGPHP	SIGRZ

– – – Four Cycles of Output are Omitted – – –

TIME = 0.60 0.21807E-04

0.800	0.	0.	0.	0.7120652E-04	-0.2193067E-04	-0.1864172E-04	-0.1866330E-04	0.
0.800	0.254	0.	0.3320824E-06	0.7120652E-04	-0.2180658E-04	-0.1851763E-04	-0.1851763E-04	0.4105088E-14
0.800	0.508	0.	0.6641648E-06	0.7159955E-04	-0.2180658E-04	-0.1847874E-04	-0.1849974E-04	-0.2838375E-13
0.800	0.762	0.	0.1319349E-05	0.7229055E-04	-0.2180658E-04	-0.1839949E-04	-0.1845306E-04	0.1782781E-13
0.800	1.016	0.	0.2583550E-05	0.7374751E-04	-0.2180658E-04	-0.1824394E-04	-0.1836196E-04	0.
0.800	1.270	0.	0.5045406E-05	0.7660826E-04	-0.2180658E-04	-0.1793612E-04	-0.1818590E-04	0.9383057E-14
0.800	1.524	0.	0.9857999E-05	0.8220555E-04	-0.2180658E-04	-0.1733264E-04	-0.1784752E-04	-0.1876611E-13
0.800	1.778	0.	0.1947034E-04	0.9320662E-04	-0.2180658E-04	-0.1614445E-04	-0.1719356E-04	0.
0.800	2.032	0.	0.3839505E-04	0.1148901E-03	-0.2180658E-04	-0.1380134E-04	-0.1592427E-04	0.1501289E-13
0.800	2.286	0.	0.7586112E-04	0.1577404E-03	-0.2180658E-04	-0.9173968E-05	-0.1345129E-04	0.
0.800	2.540	0.	0.1501077E-03	0.2425151E-03	-0.2180658E-04	-0.6821210E-12	-0.8666778E-05	0.
0.800	2.794	0.	0.2975557E-03	0.4065528E-03	-0.2616414E-03	-0.2571922E-03	-0.2360969E-03	-0.2118625E-04
0.800	0.	0.254	0.	0.2092966E-04	-0.8617329E-05	-0.7343209E-05	-0.7341847E-05	0.
0.800	0.254	0.254	-0.2094787E-07	0.2092966E-04	-0.8634475E-05	-0.7361975E-05	-0.7360354E-05	0.3167766E-08
0.800	0.508	0.254	-0.6683157E-07	0.2100745E-04	-0.8680022E-05	-0.7404462E-05	-0.7402033E-05	0.5981521E-08
0.800	0.762	0.254	-0.1376165E-06	0.2112791E-04	-0.8759358E-05	-0.7481013E-05	-0.7474923E-05	0.1275482E-07
0.800	1.016	0.254	-0.2771963E-06	0.2138908E-04	-0.8924694E-05	-0.7639412E-05	-0.7626064E-05	0.2532094E-07
0.800	1.270	0.254	-0.5518886E-06	0.2190389E-04	-0.9252496E-05	-0.7954199E-05	-0.7925553E-05	0.5060925E-07
0.800	1.524	0.254	-0.1103066E-05	0.2293497E-04	-0.9907556E-05	-0.8583540E-05	-0.8523347E-05	0.1014429E-06
0.800	1.778	0.254	-0.2213121E-05	0.2500506E-04	-0.1122065E-04	-0.9845670E-05	-0.9720507E-05	0.2040519E-06
0.800	2.032	0.254	-0.4455227E-05	0.2917509E-04	-0.1383191E-04	-0.1235012E-04	-0.1209658E-04	0.4117864E-06
0.800	2.286	0.254	-0.8913597E-05	0.3760193E-04	-0.1763233E-04	-0.1567868E-04	-0.1541703E-04	0.8226334E-06
0.800	2.540	0.254	-0.1393010E-04	0.5441318E-04	-0.6281059E-05	-0.2557954E-12	-0.3021459E-05	-0.
0.800	2.794	0.254	0.3116974E-04	0.4053570E-04	-0.2713700E-04	-0.2671103E-04	-0.2450123E-04	-0.2211174E-05
0.800	0.	0.508	0.	0.1303115E-05	-0.5608490E-06	-0.4775112E-06	-0.4778297E-06	0.
0.800	0.254	0.508	-0.1254535E-08	0.1303115E-05	-0.5615791E-06	-0.4786868E-06	-0.4786414E-06	0.2281862E-09
0.800	0.508	0.508	-0.3208581E-08	0.1308911E-05	-0.5646067E-06	-0.4814168E-06	-0.4813230E-06	0.3883936E-09
0.800	0.762	0.508	-0.6256226E-08	0.1317727E-05	-0.5698548E-06	-0.4863286E-06	-0.4860422E-06	0.8264742E-09
0.800	1.016	0.508	-0.1274747E-07	0.1337043E-05	-0.5808791E-06	-0.4965301E-06	-0.4959106E-06	0.1641616E-08
0.800	1.270	0.508	-0.2546679E-07	0.1375097E-05	-0.6027946E-06	-0.5168759E-06	-0.5155317E-06	0.3293404E-08
0.800	1.524	0.508	-0.5124459E-07	0.1451545E-05	-0.6467411E-06	-0.5576803E-06	-0.5548442E-06	0.6624674E-08
0.800	1.778	0.508	-0.1034258E-06	0.1605304E-05	-0.7350878E-06	-0.6397456E-06	-0.6338252E-06	0.1336975E-07
0.800	2.032	0.508	-0.2093007E-06	0.1915611E-05	-0.9072194E-06	-0.7982036E-06	-0.7869769E-06	0.2640927E-07
0.800	2.286	0.508	-0.4082137E-06	0.2523616E-05	-0.9693410E-06	-0.7854517E-06	-0.8115082E-06	0.2412714E-07
0.800	2.540	0.508	-0.5262501E-07	0.2862895E-05	-0.3395509E-06	-0.2486900E-13	-0.1566928E-06	-0.8356786E-15
0.800	2.794	0.508	0.2353236E-05	0.2811371E-05	-0.2013897E-05	-0.1986904E-05	-0.1820070E-05	-0.1658075E-06
0.800	0.	0.762	0.	0.2565151E-07	-0.1119531E-07	-0.9540167E-08	-0.9538321E-08	0.
0.800	0.254	0.762	-0.2841707E-10	0.2565151E-07	-0.1121130E-07	-0.9557089E-08	-0.9556155E-08	0.4951630E-11
0.800	0.508	0.762	-0.7120238E-10	0.2577566E-07	-0.1127684E-07	-0.9616134E-08	-0.9614146E-08	0.8629776E-11
0.800	0.762	0.762	-0.1374022E-09	0.2597051E-07	-0.1139429E-07	-0.9726004E-08	-0.9719680E-08	0.1835581E-10
0.800	1.016	0.762	-0.2805216E-09	0.2639893E-07	-0.1164115E-07	-0.9954111E-08	-0.9940476E-08	0.3643099E-10
0.800	1.270	0.762	-0.5604521E-09	0.2724146E-07	-0.1213144E-07	-0.1040872E-07	-0.1037911E-07	0.7316279E-10
0.800	1.524	0.762	-0.1128160E-08	0.2893636E-07	-0.1311559E-07	-0.1132127E-07	-0.1125880E-07	0.1472166E-09
0.800	1.778	0.762	-0.2277481E-08	0.3234637E-07	-0.1507490E-07	-0.1313393E-07	-0.1300693E-07	0.2965653E-09
0.800	2.032	0.762	-0.4556968E-08	0.3921099E-07	-0.1746517E-07	-0.1495999E-07	-0.1496962E-07	0.4847425E-09
0.800	2.286	0.762	-0.4978412E-08	0.4959829E-07	-0.2038502E-07	-0.1692900E-07	-0.1721693E-07	-0.2389779E-10
0.800	2.540	0.762	-0.1101024E-08	0.4389328E-07	-0.5263597E-08	-0.1110223E-15	-0.2431702E-08	-0.2748943E-17
0.800	2.794	0.762	0.3620681E-07	0.4278301E-07	-0.3097223E-07	-0.3055893E-07	-0.2799203E-07	-0.2555649E-08
0.800	0.	1.016	0.	0.1544618E-09	-0.6782617E-10	-0.5780006E-10	-0.5778807E-10	0.
0.800	0.254	1.016	-0.1845971E-12	0.1544618E-09	-0.6793366E-10	-0.5791425E-10	-0.5790755E-10	0.3246980E-13
0.800	0.508	1.016	-0.4722516E-12	0.1552765E-09	-0.6837080E-10	-0.5830897E-10	-0.5829510E-10	0.5845880E-13
0.800	0.762	1.016	-0.9218614E-12	0.1566033E-09	-0.6916997E-10	-0.5905506E-10	-0.5901267E-10	0.1248487E-12
0.800	1.016	1.016	-0.1881395E-11	0.1595237E-09	-0.7085461E-10	-0.6060949E-10	-0.6051811E-10	0.2473834E-12
0.800	1.270	1.016	-0.3757850E-11	0.1652555E-09	-0.7419540E-10	-0.6370324E-10	-0.6350469E-10	0.4969712E-12
0.800	1.524	1.016	-0.7564685E-11	0.1767920E-09	-0.8090316E-10	-0.6991463E-10	-0.6949581E-10	0.9998141E-12
0.800	1.778	1.016	-0.1527C06E-10	0.1999967E-09	-0.9265739E-10	-0.8037494E-10	-0.7980185E-10	0.1827727E-11
0.800	2.032	1.016	-0.2626993E-10	0.2409751E-09	-0.1004293E-09	-0.8363757E-10	-0.8498234E-10	0.2644689E-11
0.800	2.286	1.016	-0.8860888E-11	0.2960958E-09	-0.1234864E-09	-0.1030667E-09	-0.1043078E-09	-0.2599399E-11
0.800	2.540	1.016	0.9252912E-11	0.2072381E-09	-0.2488934E-10	-0.1084202E-17	-0.1136130E-10	-0.2863482E-19
0.800	2.794	1.016	0.1850009E-09	0.2164910E-09	-0.1578136E-09	-0.1557671E-09	-0.1426513E-09	-0.1304600E-10
0.800	0.	1.270	0.	0.	0.	0.	0.	0.
0.800	0.254	1.270	0.	0.	0.	0.	0.	0.
0.800	0.508	1.270	0.	0.	0.	0.	0.	0.
0.800	0.762	1.270	0.	0.	0.	0.	0.	0.
0.800	1.016	1.270	0.	0.	0.	0.	0.	0.
0.800	1.270	1.270	0.	0.	0.	0.	0.	0.
0.800	1.524	1.270	0.	0.	0.	-0.	0.	-0.
0.800	1.778	1.270	-0.	-0.	0.	-0.	-0.	0.
0.800	2.032	1.270	-0.	0.	-0.	0.	-0.	0.
0.800	2.286	1.270	0.	0.	-0.	0.	0.	-0.
0.800	2.540	1.270	0.	-0.	0.	-0.	0.	-0.
0.800	2.794	1.270	-0.	-0.	0.	0.	-0.	0.

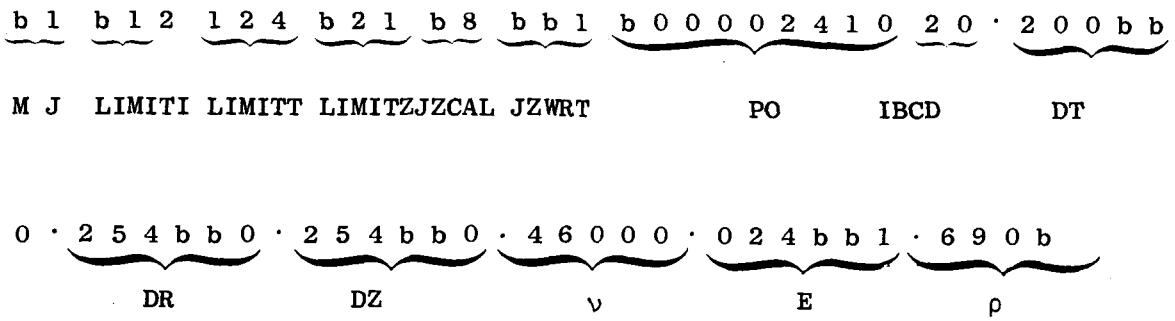
b 1 b 1 2 1 2 4 b 2 1 b 8 b b 1 b 0 0 0 0 0 2 4 1 0 2 0 · 2 0 0 b b
M J LIMITI LIMITT LIMITZJZCAL JZWRT PO IBCD DT
0 · 2 5 4 b b 0 · 2 5 4 b b 0 · 4 6 0 0 0 · 0 2 4 b b 1 · 6 9 0 b
DR DZ ν E ρ

NOTES AND DEFINITIONS

Input data (cards 005-007)

MM is the number of time increments the program computes before output is again obtained.

LIMITI is the number of radial zones.

LIMITT is the total number of time increments.

LIMITZ is the number of axial zones.

JZCAL is the approximate number of axial increments that are computed beyond the front of the wave.

JZWRT is the number of axial increments the program computes before output is again obtained.

PO is the magnitude of the step in pressure at z = 0.

IBCD either equals 1 or 2

IBCD = 1 for a free end at z = L
IBCD = 2 for a fixed end at z = L

XNU is the Poisson ratio (ν).

Frequently used constants (cards 008-016)

Output formats (cards 017-031)

These statements produce the output shown at the top of page 10.

Set initial conditions (cards 032-036)

Time base (cards 038-039)

TIME = FM*DT

Pressure condition (cards 040)

Any arbitrary time dependence of the applied pressure (PO) at z = 0 can be inserted here.

Equations of motion (cards 043-066)

Cards 048-066 are equations (40) of Bertholf's thesis.

Boundary conditions (cards 074-177)

JJ is the largest number of axial increments for which boundary conditions are necessary.

Cards 078-082 are the r = 0 conditions for proper behavior.

Cards 084-088 are the boundary conditions for a fixed end at z = L. These are equations (88) and (89) of Bertholf's thesis.

Cards 091-129 are the boundary conditions for a free end at z = L. These are equations (86) of Bertholf's thesis. This option has not been used in the present computation. These equations are rewritten in the following system:

$$(AA)\ (XX) = (BB)$$

where XX(I) is defined as shown in cards 122-125. This linear system is solved by using the subroutine SSOLVE.*

Cards 131-165 are the boundary conditions for a pressure at z = 0. These are equations (80) and (81) of Bertholf's thesis which are rewritten in the system (A) (X) = (B). The method is the same as used for a free end at z = L. In fact, the same subroutine was used with a different name--SOLVE. This is done so that the inverse for each matrix can be calculated and stored separately.

Cards 166-173 are the boundary conditions at r = R. These cards are equations (44) of Bertholf's thesis.

Reset initial conditions (cards 178-184)

Output statements (cards 185-198)

These statements yield the values shown on the output pages included immediately after the program listing.

---

*SSOLVE is a suitable adaptation of SOLVE. It was not used in the computation described here.

INC (see card 075) is the number of radial increments the program computes before output is again obtained. For INC = 11, only the surface values are given in the output. For INC = 1, values are printed for all R.

U(R(is radial displacement at (r,z,t)

W(R) is axial displacement at (r,z,t)

SIGZZ = σ_{zz}

SIGRR = σ_{rr}

SIGPHP = $\sigma_{\varphi\varphi}$

SIGRZ = σ_{rz}

σ_{zz}, etc. are components of the stress matrix at (r,z,t), positive in tension.